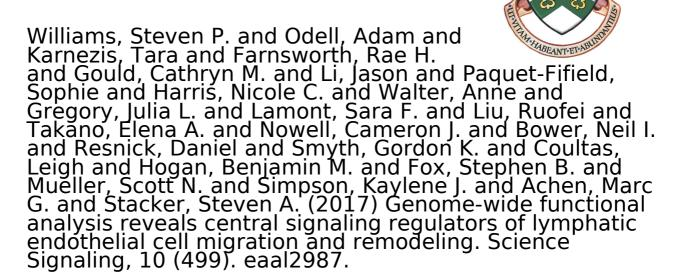
# York St John University



Downloaded from: http://ray.yorksj.ac.uk/id/eprint/2933/

The version presented here may differ from the published version or version of record. If you intend to cite from the work you are advised to consult the publisher's version:

https://doi.org/10.1126/scisignal.aal2987

Research at York St John (RaY) is an institutional repository. It supports the principles of open access by making the research outputs of the University available in digital form. Copyright of the items stored in RaY reside with the

RaY

Research at the University of York St John

For more information please contact RaY at <a href="mailto:ray@yorksj.ac.uk">ray@yorksj.ac.uk</a>

One-sentence summary: The signaling proteins and pathways involved in lymphatic endothelial cell migration are identified.

**Comment [WW1]:** WW to authors: This must be a complete sentence and cannot be a phrase.

#### **Editor's summary:**

### Moving lymphatic endothelial cells about

Lymphatic vessels return fluid and immune cells from peripheral tissues back to the circulation. The growth of new lymphatic vessels and their remodeling are critical for clearing infection and for metastasis of many cancer subtypes. Williams *et al.* compared the results of their functional siRNA screens with previously published mRNA datasets to identify genes that regulated lymphatic endothelial cell migration, a process critical for lymphatic vessel growth and remodeling, and genes that functioned in both lymphatic and blood endothelial cell migration. One of the top candidates to emerge from these analyses, the glycan-binding protein Galectin-1, not only promoted lymphatic vessel growth, but was also important for maintaining lymphatic endothelial cell identity. Further analyses of the authors' results may reveal lymphatic vessel–associated proteins that could be targeted to prevent edema, improve infection outcomes, or limit metastasis.

# Genome-wide functional analysis reveals central signaling regulators of lymphatic endothelial cell migration and remodeling

Steven P. Williams \(^{1,6,9,\*}\), Adam F. Odell \(^{1,5,\pmu}\), Tara Karnezis \(^{1,5,^\check}\), Rae H. Farnsworth \(^1\), Cathryn M. Gould \(^2\), Jason Li \(^{4,5}\), Sophie Paquet-Fifield \(^{1,5,+}\), Nicole C. Harris \(^{1,6,9,^\check}\), Anne Walter \(^{10}\), Julia L. Gregory \(^{10}\), Sara F. Lamont \(^{1,11}\), Ruofei Liu \(^{1,5}\), Elena A. Takano \(^3\), Cameron J. Nowell \(^{9,12}\), Neil I. Bower \(^{15}\), Daniel Resnick \(^{1,9}\), Gordon K. Smyth \(^{8,13}\), Leigh Coultas \(^{7,14}\), Benjamin M. Hogan \(^{15}\), Stephen B. Fox \(^{1,3}\), Scott N. Mueller \(^{10}\), Kaylene J. Simpson \(^{2,5}\), Marc G. Achen \(^{1,5}\) and Steven A. Stacker \(^{1,5,\beta}\)

<sup>¶</sup> Equal first authors

<sup>&</sup>lt;sup>1</sup>Tumour Angiogenesis and Microenvironment Program,

<sup>&</sup>lt;sup>2</sup>Victorian Centre for Functional Genomics,

<sup>&</sup>lt;sup>3</sup>Department of Pathology,

<sup>&</sup>lt;sup>4</sup>Bioinformatics Core.

Peter MacCallum Cancer Centre, Melbourne, Victoria 3000, Australia

University of Melbourne, Parkville, Victoria 3010, Australia.

<sup>9</sup>Ludwig Institute for Cancer Research, Royal Melbourne Hospital, Parkville, Victoria 3050, Australia.

<sup>10</sup>Department of Microbiology and Immunology, The University of Melbourne, at the

Peter Doherty Institute for Infection and Immunity, Melbourne 3000, Australia

<sup>11</sup>Department of Biochemistry and Genetics, La Trobe Institute for Molecular Sciences,

La Trobe University, Bundoora, Victoria 3086, Australia.

<sup>12</sup>Centre for Dynamic Imaging, Systems Biology and Personalised Medicine Division,

The Walter and Eliza Hall Institute of Medical Research, Parkville, Victoria 3052,

Australia.

<sup>15</sup>Division of Genomics of Development and Disease, Institute for Molecular Bioscience,

The University of Queensland, Brisbane, Queensland 4072, Australia

\*Current address: Cancer Functional Genomics, Wellcome Trust Sanger Institute,

Wellcome Trust Genome Campus, Hinxton, CB10 1SA, UK

\*Current address: Faculty of Medicine and Health, University of Leeds, Leeds, LS9 7TF,

<sup>&</sup>lt;sup>5</sup>Sir Peter MacCallum Department of Oncology,

<sup>&</sup>lt;sup>6</sup>Department of Surgery, Royal Melbourne Hospital,

<sup>&</sup>lt;sup>7</sup>Department of Medical Biology,

<sup>&</sup>lt;sup>8</sup>Department of Mathematics and Statistics

<sup>&</sup>lt;sup>13</sup>Bioinformatics Division,

<sup>&</sup>lt;sup>14</sup>Development and Cancer Division,

UK.

<sup>^</sup>Current address: O'Brian Institute of Microsurgery, Department of St Vincent's Institute of Medical Research, Fitzroy, Victoria 3065, Australia.

<sup>+</sup>Current address: Department of Pathology, University of Melbourne, Parkville, Victoria 3010, Australia.

§Correspondence should be addressed to: Steven A. Stacker;

email: <a href="mailto:steven.stacker@petermac.org">steven.stacker@petermac.org</a>, phone: +61-385597106, Peter MacCallum Cancer Centre, 305 Grattan Street, Melbourne Victoria 3000, Australia

# **Abstract**

Lymphatic vessels constitute a specialized vasculature that is involved in development, cancer, obesity and immune regulation. The migration of lymphatic endothelial cells (LECs) is critical for vessel growth (lymphangiogenesis) and vessel remodelling, processes that modify the lymphatic network in response to developmental or pathological demands. Using the publicly accessible results of our genome-wide siRNA screen, we characterized the migratome of primary human LECs and identified individual genes and signaling pathways that regulate LEC migration. We compared our dataset with mRNA differential expression data from endothelial and stromal cells derived from two in vivo models of lymphatic vessel remodeling, viral infection and contact hypersensitivity-induced inflammation, which identified genes selectively involved in regulating LEC migration and remodeling. We also characterized the top candidates in the LEC migratome in primary blood vascular endothelial cells to identify genes with functions common to lymphatic and blood vascular endothelium. Based on these

analyses, we showed that *LGALS1*, which encodes the glycan-binding protein Galectin-1, promoted lymphatic vascular growth in vitro and in vivo and contributed to maintenance of the lymphatic endothelial phenotype. Our results provide insight into the signaling networks that control lymphangiogenesis and lymphatic remodeling and potentially identify therapeutic targets and biomarkers in disease specific to lymphatic or blood vessels.

**Comment [WW2]:** WW to authors: Had to remove "resource" for administrative purposes.

# Introduction

The lymphatic vasculature is a unidirectional system of vessels with essential roles in normal and pathological physiology. The endothelial cells (ECs) lining lymphatic vessels regulate many of these functions, including fluid resorption, secretion of proteins into lymph fluid (*I*), and interaction with immune cells (2). Sprouting growth (lymphangiogenesis) and remodelling of lymphatic vessels are essential during both embryonic development of the differentiated lymphatic vasculature and in adult pathological contexts such as wound healing, inflammation, immune responses and cancer (*3*, *4*). During immune responses, growth and remodelling of lymphatics at the primary site and its draining lymph node (LN) enhance trafficking of dendritic cells, with implications for generating effective antigen-specific immune responses (*2*, *3*). In cancer, however, increased lymphatic vessel density in tumours is correlated with disease progression and decreased survival (*4*), indicating that expansion of the lymphatic vasculature enables metastatic spread of tumour cells to the draining LNs and potentially to distant organs (*1*, *5*, *6*). The sprouting growth, remodelling, and early developmental separation and differentiation of lymphatics, all require coordinated migration of

lymphatic endothelial cells (LECs) (7, 8).

Cell migration requires the complex coordination of multiple individual processes within and between cells (9, 10), including extension and depolymerisation of actin- and tubulincomprised cytoskeletal structures, formation and vesicular recycling of adhesion complexes, and regulatory signal transduction in response to guiding stimuli. To better understand the complex signalling networks regulating cell migration, and to discover previously unidentified components, several groups have conducted RNA interference screens in various cell types using the scratch wound assay of collective cell migration (11-15). Whilst these studies have successfully identified genes and signalling networks that regulate cell migration in vitro, the findings are not often validated in diverse experimental systems, and the relevance of these findings to human disease is rarely directly explored. Although various signalling pathways have been identified as key drivers of LEC migration through various experimental systems, including the vascular endothelial growth factor (VEGF) pathways involving VEGFC, VEGFD, VEGFR3 and Neuropilin 2 (NRP2) (8, 16-19), the broader lymphatic endothelial "migratome" remains unmapped and represents an untapped pool of potential therapeutic targets for controlling lymphangiogenesis.

Here we describe an unbiased siRNA functional screening approach aimed at understanding the LEC migratome. As well as successfully identifying genes that have already been linked to cell migration or vascular development, the screen also identified genes not previously associated with cell migration or lymphatic biology. Knockdown of the validated gene set in blood vascular endothelial cells (BECs) identified subsets of genes that had either common or distinct roles in each EC type. Comparison with

microarray data derived from two in vivo models of lymphatic growth and remodelling confirmed the biological relevance of several of these genes and the screen globally. Futhermore a particular candidate, *LGALS1* (encoding Galectin-1; Gal-1), played a role in regulating lymphangiogenesis and LEC phenotype. This study provides insight into the signalling networks that control the migration of both lymphatic and blood vascular ECs, and has identified a pool of potential new therapeutic targets.

### **Results**

A genome-wide siRNA screen identifies high confidence genes required for LEC migration.

To identify genes and signalling pathways that regulate migration of LECs we have conducted a genome-wide siRNA functional screen involving 18,120 SMARTpools targeting protein-coding genes using primary human dermal microvascular neonatal lymphatic endothelial cells (HDLECs) (fig. S1, A to C; Data File S1). We have published a technical description of this screen and deposited the datasets in publicly accessible databases (20). Using high-throughput cell culture robotics, microscopy and image analysis, this screen measures the migration of siRNA-transfected HDLECs into a scratch wound created in the cell monolayer (15) (Fig. 1A; fig. S1, D to G; S2, A to F; S3). Genes that impair cell proliferation and viability rather than migration are identified using nuclear counting, and 438 genes classified as "Low Cell Count" are thus excluded from further analysis in the migration screens (Fig. 1B). This list included *FLT4*, encoding VEGFR3, which is central for LEC growth and survival, as well as several genes encoding other growth factor receptors and key downstream signalling kinases such as

### *PI3K*.

Quantification of the wound area covered by migrating cells after 24 hours (fig. S2, E and F) relative to mock-transfected controls provides an index of cell migration capacity, which is then normalized to generate z scores (21). A threshold of |robust z score| >2 (a robust z score >2 or <-2, representing the top and bottom 2.3% of scores) is used to identify biologically and statistically relevant candidate genes for further rounds of screening (20). Consequently a total of 650 genes have been classified with regard to siRNA-mediated migration outcome as "Impaired" (robust z score <-2), and 385 as "Accelerated" (robust z score >2; Fig. 1B).

To technically validate the results of the primary screen 500 candidate genes have been analysed in a secondary screen in which the four component siRNAs of the SMARTpools are assayed individually (20). The list comprises 401 "Impaired" and 99 "Accelerated" candidates, curated according to highest robust z scores, greater expression in lymphatic than in blood endothelium, and protein-protein interactions with the products of other candidate genes. The greater representation of "Impaired" compared to "Accelerated" candidates reflected the higher representation of the "Impaired" phenotype in the primary screen, and our focus on identifying positive regulators of HDLEC migration (knockdown of which would generate an "Impaired" phenotype). The secondary screen has validated 154 genes with medium to high confidence (with 2-4 duplexes reproducing the primary screen phenotype) (Data File S2). All of these candidates impair cell migration when knocked down. For a further 5 "Accelerated" and 117 "Impaired" candidates from the primary screen, the original phenotype was reproduced unambiguously by only 1 of the 4 individual siRNAs (Data File S2); these genes were

considered to be validated with low confidence. The higher rate of validation for "Impaired" than "Accelerated" phenotypes highlighted the selectivity of our assay system for identifying positive regulators of HDLEC migration, but may also indicate that relatively more genes expressed in HDLECs function to promote than to restrict migration.

To determine the biological relevance of the genes identified in the first two stages of the siRNA screen, we subsequently assessed the data at multiple levels to identify important genes and signalling networks (Fig. 1C). At the most stringent level, the 154 genes validated in the secondary screen – the "highly-validated" migration candidates – were carried forward into a tertiary screen to assess their effects on cell morphology and in blood vascular ECs, as well as more detailed functional cell biological analyses. The 1035 genes with |robust z score| >2 in the primary screen - the "migration candidates" – provided a broader analysis of signalling pathway and gene ontology (GO) enrichment. Finally, the "expanded migration candidate" gene set, including all genes from the primary screen with |robust z score| ≥1.6449 (representing the top 5% and bottom 5% of robust z scores), was used for comparison to independent in vivo-derived datasets.

Candidate migration genes in lymphatic endothelium are associated with EC biology, migration and key signalling networks.

Signalling pathway enrichment analysis of the "migration candidates" (|robust z score| >2) showed that these were significantly over-represented in pathways related to cytoskeleton remodelling and development (Data File S3). Analysis of gene ontology (GO) processes also revealed over-representation of genes assigned to terms such as

"regulation of endothelial cell migration" and "regulation of positive chemotaxis", as well as terms broadly associated with phosphorylation and signalling (Data File S4). The range of impaired migration phenotypes indeed suggested that multiple different cell processes had been perturbed (fig. S1G).

We grouped the "highly-validated" migration candidate genes into functional categories based on GO terms and previous studies describing their known or proposed role in the cell using the Metacore database (Fig. 2). Mapping to GO processes showed that many of these 154 candidates were linked to specifically relevant terms such as "locomotion" (~23% of the candidates), "response to wounding" (~23%), "cell migration" (~17%) and "vasculature development" (~15%) (Data File S5). Enrichment analysis also revealed statistically significant over-representation in pathways linked to cytoskeleton remodelling, cell adhesion and VEGF-driven signalling cascades (fig. S4, Data File S6). Ten "highly-validated" HDLEC migration genes had been previously associated with canonical aspects of cytoskeletal remodelling or migration pathways (AKT3, GNAS, IL1B, JUN, LIMK1, PDGFRB, PLCG1, MYL7, CALM2 and CDC42; Data File S6). Developmental signalling pathways were also over-represented, including signalling cascades downstream of FGF and PDGF receptors and growth hormone and erythropoietin (EPO) signalling pathways, which have been previously reported to be important for lymphatic vessel growth (22, 23). The receptor tyrosine kinase PDGFRβ and the growth factor ANGPT2 have also been defined as regulators of lymphangiogenesis (24, 25), thus further emphasizing the ability of the screen to identify biologically relevant genes.

Other signalling pathways over-represented in the "highly-validated" gene set included

those connected to directed migration of neuronal sprouts (axon guidance); and the immune response, reflecting the interconnectedness of lymphatic remodelling and immunity (Data File S6). Components of inositol phosphate and glycerophospholipid metabolism pathways were also enriched (Fig. 2 and fig. S4), supporting the importance of these molecules in signalling pathways leading to cell migration (26).

# Morphology analysis gives insight into function of highly-validated genes in cell migration.

The process of cell migration affects cell morphology due to dynamic remodelling of the cytoskeleton and regulation of cell-substrate adhesion (10, 14). To gain further insight into the specific subcellular functions of the 154 "highly-validated" migration candidate genes, images of the respective siRNA-transfected cells have been analysed in a tertiary screen to assess various cellular and cytoskeletal parameters, including area and other dimensional measurements (indicative of cell-substrate adhesion and spreading), cell shape (reflecting spreading or lateral polarisation), average actin intensity (reflecting overall abundance of filamentous actin) and actin texture (variability in intensity, reflecting discrete actin structures) (Fig. 3, A and B) (20). Distinct morphological changes in siRNA-transfected HDLECs were visibly evident in images of the cell monolayers 24 h post-wounding (Fig. 3C, fig. S5A). Hierarchical clustering of the normalized morphology parameter datasets has identified six clusters of gene-specific siRNA SMARTpools that induce similar morphological phenotypes (Fig. 3, B and D; fig. S5A and B; Data File S2).

Silencing of genes in cluster 1 did not significantly alter HDLEC morphology compared

to mock transfected cells, suggesting that proteins such as PIK4A and PIK4B (Fig. 3D; Data File S2) regulate HDLEC migration in ways that do not influence morphology. In contrast, knockdown of genes such as IL1B, MICAL2, GPR84 and LGALS1 in cluster 2 led to cells that were more elongated, and had increased and uniform actin staining (Fig. 2, B to D; Data File S2). Galectin-1 (encoded by LGALS1) disturbs the integrity of the cortical cytoskeleton (involving a decrease in VE-cadherin-mediated cell-cell junctions) and promotes stress fibre formation in HUVECs by binding to NRP1 at the cell membrane and activating downstream Rho kinase signalling (27). A similar mechanism in HDLECs may explain the diffuse actin staining pattern typical of knockdown of genes in this cluster. Cluster 2 also included HOXC5, which encodes a transcription factor, PLCG1 and BTK (Fig. 3B to D; Fig. S5A, Data File S2). BTK and PLCγ2 regulate chemokine-controlled, integrin-mediated migration in B lymphocytes (28, 29), which likely involves the ability of BTK to promote actin nucleation and polymerization (30). The inhibition of this pathway in our HDLEC screen may thus be responsible for the observed migration and morphology phenotypes. Notably, knockdown of genes in cluster 2 also resulted in significantly more impaired migration compared to knockdown of those in cluster 1, which did not alter morphology, thus highlighting the connection between cell morphology and migration (fig. S5C).

Targeting of genes in cluster 6 led to cells that were more elongated, but also larger in area than control cells. This phenotype was characteristic of siRNA SMARTpools targeting *CDC42* and the gene encoding the downstream kinase LIMK1 (Fig. 3, B and D; fig. S5A). Similarly, silencing of genes in cluster 3 such as *ANGPT2* and *EPOR* led to larger cells with low average actin staining (Fig. 3, B and D; fig. S5A). ANGPT2

regulates developmental lymphatic migration and remodelling (25, 31), and triggers stress fibre formation at the expense of cell-cell junction integrity in BECs by activating integrin-β1 (32). EPOR (EPO receptor) can induce lymphangiogenesis when activated by EPO (23) or potentially through transactivation by VEGFA-activated VEGFR2 as is shown in blood vascular endothelium (33). Other genes that clustered with this phenotype included carbohydrate sulfotransferases (CHST5, CHST8), cytoskeleton interacting proteins (FLCN, MYL7, and TUBA1B), and several uncharacterized genes not previously known to regulate cell morphology (C2orf28, C7orf55, C17orf59, C11orf63). Knockdown of genes in cluster 5 (which included SETD2 and KANSL1), increased cell area but did not affect actin intensity or distribution (Fig. 3B and D; fig. S5A). SETD2 is a histone H3 lysine 36 methyltransferase that has been implicated in remodelling of the embryonic vasculature (34). KANSL1 is also a component of a histone acetyl transferase complex (35), suggesting that these factors may control the expression of suites of genes involved in regulating EC size and migration. Lastly, knockdown of genes in cluster 4 such as TPST2, RTKN and JUN led to elongated cells, with lower intensity actin staining but higher texture difference of actin staining, potentially indicating stress fibre formation (Fig. 3B and D; fig, S5A). TPST2 encodes a tyrosylprotein sulfotransferase that is activated in ECs under shear stress conditions (36), while RTKN regulates actin remodelling pathways by inhibiting the GTPase activity of Rho family proteins (37). JUN encodes the AP-1 transcription factor subunit c-Jun, which is annotated to multiple signaling pathway and processes related to cell migration (Data Files S3 and S6). For example, it promotes sheet migration of epithelial cells through inducing transcription of pro-migratory factors such as EGF (38).

Screening of BEC migration reveals common regulators of EC migration and identifies distinct migration machinery in LECs.

To understand the conservation of functional pathways between different EC types, the "highly-validated" migration candidates have been reassessed in a tertiary siRNA screen for migration effects in both human microvascular blood endothelial cells (HMBECs) and HDLECs (Fig. 4A) (20). To minimise differences due to vessel calibre or anatomical location, HMBECs isolated from neonate dermis are used to match the source of the HDLECs. HMBECs lacked the LEC molecular markers PROX1, Podoplanin and LYVE1 but produced more von Willebrand factor (fig. S6A; compare to fig. S1, B and C) (39). The migration of primary HMBECs in the scratch wound assay was faster than HDLECs, such that the wound was 50% closed after 16 h (fig. S6B).

The similarity of the siRNA target-specific phenotypes between the two cell types was high, despite the difference in wound closure dynamics. Using a cut-off of <65% of mock-transfected cell migration, 111 of the 154 siRNA pools have resulted in impaired migration in at least one cell type (Fig. 4A). The comparison demonstrated that while a substantial portion (61.3%) of the gene candidates derived from the genome-wide HDLEC migration screen also affected HMBEC migration, a subset had cell-type specific effects (Fig. 4, A and B; Fig. S7, A to C). Analysis of the HMBEC migration screen results allowed grouping of candidate genes into 68 "Common EC" migration genes important for the migration of both EC types, 23 "BEC dominant" genes with a greater effect on the migration of HMBECs, and 20 "LEC dominant" genes with a greater effect on HDLECs (Fig. 4, A and C, Data File S2).

The morphological attributes of the siRNA-transfected HMBECs largely resembled those of the HDLECs (Fig. 4D, compare to Fig. 3B). This result not only confirmed the robustness of the morphological changes observed, but further emphasized the functional importance of these genes for both cell types. The clustering of genes with similar morphological phenotypes suggested possible inter-connected signalling pathways controlling specific aspects of cytoskeletal remodelling and cell migration. However, there were also some differences between the morphologies caused by gene silencing in HMBECs and HDLECs (Fig. 4, C to E; fig. S7, A to C). For example, silencing of SGK3 in HMBECs caused an increase in cell size and elongation that was not seen in HDLECs (fig. S7, A and C) and inhibited migration more strongly than in HDLECs (Fig. 4C). Silencing of CDC42 in HMBECs did not result in a decreased shape factor (namely elongation; fig. S7, B to C). This finding supported the increased impairment of migration by CDC42 silencing in HDLECs compared to HMBECs (Fig. 4, B and C; Data File S2), emphasizing the differential function of this protein in the different cell types. Assessment of lymphatic (CEACAM-1, identified by microarray analysis as HDLEC enriched) and blood (CD146) EC marker abundance after depletion of CDC42 or LIMK1 confirms the linkage of these differential effects to each distinct cell lineage (fig. S7D). LPL siRNA also led to impaired migration and elongated morphology (reduced shape factor) in HDLECs but not in HMBECs (Fig. 4, C to E). Lipoprotein lipase (LPL) is important for the hydrolysis of lipoproteins (for example low-density lipoprotein) to fatty acids, and their uptake into cells (40). This cell-type specific effect may reflect the important role that the lymphatics play in absorption of fatty acids from the gut, and a role for LPL in LEC migration could relate to the association between lymphatic function

and fat deposition (1). Knockdown of LPL inhibits migration of glioma cells (41), an effect that may relate to its interaction with heparan sulfate proteoglycans that are closely linked with components of the actin cytoskeleton (42). Furthermore exogenous LPL regulates inflammatory responses in a crtic ECs, suppressing TNF $\alpha$ -induced gene expression by activation of I $\kappa$ B $\alpha$  whilst enhancing IFN $\gamma$ -induced gene expression (43).

Identification of genes involved in LEC migration enables construction of a migration signalling network.

To better understand the molecular mechanisms required for EC migration, we utilized a protein–protein interaction database (Metacore) to map the signalling pathways of the genes identified in our screen. Construction of a signalling network using both "Common EC" migration genes and "LEC dominant" genes demonstrated that many of these proteins were closely connected (Fig. 5). Indeed, some of these molecules were key nodes of the EC migratome network (such as PLCG1, JUN, and PDGFRB). The network also revealed connections with various proteins associated with predominant migration phenotypes in HDLECs. These included CDC42, PPP1CA and BTK, which were identified as LEC nodal signalling points, suggesting that they may play central roles in coordinating migration signalling in LECs. The network also provided insight into antimigratory signalling pathways. While much of the positive signalling (Fig. 5, green lines) converged on PLCG1, CDC42 and PPP1CA, inhibitory signals (Fig. 5, red lines) passed through GSK3B. Indeed, this is consistent with the role of GSK3B as an inhibitor of key cellular functions such as protein translation and motility (44).

Candidate genes identified by siRNA screening overlap significantly with genes differentially expressed during lymphatic remodelling in vivo.

We next sought to validate that our functional in vitro siRNA screen had identified genes that were also relevant in pathological lymphangiogenesis in vivo. To this end, we compared the primary siRNA screen results to a list of genes that are differentially expressed in remodelling lymphatic endothelium from an in vivo model of viral infection (45). Sprouting growth and remodelling of both lymphatic and blood vascular networks in LNs downstream of an infection site is integral to supporting effective immune responses (3, 45). LECs, BECs and fibroblastic reticular cells (FRCs) are freshly isolated from LNs six days after cutaneous infection with Herpes Simplex Virus (HSV)-1 and their expression profiles as determined by microarray analysis compared to those of equivalent cell populations from uninfected (day 0) controls (45). We further applied a fold-change threshold (day 6 compared to day 0) of  $\geq |1.8|$  to enrich for genes whose mRNA abundance had changed to a degree that would suggest a functional biological consequence. The "expanded migration candidate" list from the siRNA screen (|robust z score| ≥ 1.6449) was selected for comparison to the microarray results. siRNA targets with a robust z score of 1.6449 in the primary screen had migration scores approximating 145% of the median ("Accelerated"), whilst a robust z score of -1.6449 corresponded to migration scores of ~55% of the median ("Impaired"). Genes classified as "Low Cell Count" were excluded as previously to focus the analysis on genes involved in migration. This expanded list was generated to potentially enable retrieval of candidates for which the conditions of the in vitro assay did not capture maximal functional impairment, and to accommodate differences in species, timeframe, stimulation factor and output

measurement between the two experimental systems.

Five days after infection, all cell subpopulations in the LN had expanded, and lymphatic growth and remodelling were evident (Fig. 6A) (45). The list of genes differentially-expressed in LN LECs at day 6 (both increased and decreased in day 6 compared to day 0 LNs) was tested for size and significance of overlap with the "expanded migration candidate" list from our migration screen using simulated null distributions (Fig. 6B) and hypergeometric distributions. This analysis revealed a statistically significant overlap of 133 genes common to the siRNA screen and LN microarray results (Fig. 6, B and C; D, row labelled "LEC total"; Data File S7). These included several genes validated in the secondary and tertiary siRNA screens, including *LGALS1*, *COPB2*, and *ANGPT2*. The statistical significance of this overlap was supported by the more conservative estimates given by hypergeometric analysis (Fig. 6D). A similar analysis of genes commonly differentially regulated in both LN LECs and BECs showed a significant overlap of 20 genes (Fig. 6D, "EC-common total"; Data File S7).

To better determine the ability of the siRNA screen to identify genes selectively involved in LEC migration, the microarray data was filtered to create lists of genes selectively differentially-expressed in LECs, BECs and FRCs. Genes were designated as "selective" for a given cell type or types (with reference to the day 6 timepoint and the three cell types analysed) if they were significantly differentially-expressed over the 1.8-fold threshold only in that cell type or types whilst being unchanged or differentially-expressed in the opposite direction in the other cell types. Lists of EC-selective differentially-expressed genes (those differentially-expressed in both BECs and LECs but not FRCs); and genes differentially expressed in all cell types (Fig. 6D) were derived

according to the same criteria. The LEC-selective differentially-expressed gene list overlapped significantly with the "expanded migration candidate" list, revealing 90 genes that were identified above the respective thresholds in both experiments (Fig. 6, D and E; Data File S7). This included "highly-validated" genes such as EPOR, SMURF2 and USP25, mapped within the LEC migration signalling network (Fig. 5), and MICAL2, a less extensively characterised gene. Comparison of the siRNA screen results to ECselective differentially-expressed genes also revealed a statistically significant overlap (Fig. 6D and E). In contrast, overlap with BEC-selective gene lists and genes commonly regulated in all cell types was not statistically significant (Fig. 6D). As additional validation, we used the same method to compare the expanded migration candidate list to an independent publicly-available microarray dataset derived from mouse ear dermal LECs in a model of contact hypersensitivity (CHS; 46). In this model, mice are first sensitised to oxazolone, then a CHS (delayed-type hypersensitivity) reaction is induced by topical application of oxazolone to the ears. This treatment results in expansion and remodelling of the lymphatic network at the site of the second oxazolone challenge, beginning within 24 hours (47). The list of genes that were differentially-expressed in CHS-activated compared to unstimulated LECs 24 hours postchallenge also overlapped significantly with our expanded migration candidate list (Fig 6F; Data File S8). Il1b mRNA was highly increased in expression in CHS-derived LECs, and its human ortholog was an EC common migration candidate (Fig. 5; Data File S8). IL1B is an inflammatory cytokine which induces cell-surface presentation of leukocyte adhesion molecules and impaired barrier function in LECs (48, 49). Furthermore IL1B may indirectly promote lymphangiogenesis by increasing autocrine or paracrine

production of VEGFC or VEGFA, and VEGFR2 in endothelium (50, 51). Overall, these analyses further validate the biological relevance of the siRNA screen by illustrating its selective ability to identify genes with enriched importance in LECs, and confirming that these genes are implicated by other methods in pathological lymphatic remodelling in vivo, both in dermal settings and in other relevant tissues.

# In vitro and in vivo assays of lymphangiogenesis and lymphatic remodelling identify Galectin-1 as a regulator of LEC function and phenotype

We next sought to confirm the role of our "highly-validated" migration candidates in LEC migration, remodelling and lymphangiogenesis. *LGALS1* and *MICAL2* (microtubule associated monoxygenase, calponin and LIM domain containing 2) were also identified in the LN remodelling microarray analysis, and exhibited the highest fold-change in expression in LECs (with the exception of the well-characterised *ANGPT2*). *MICAL2* served as a representative candidate that was selectively differentially-expressed in LECs in the LN microarray analysis, whereas *LGALS1* was the only "highly-validated" gene differentially-expressed in both LN EC types (Data File S7).

Galectins are a family of widely-distributed, secreted glycan-binding proteins with roles in regulating cell-cell adhesion and signalling in diverse biological processes, including angiogenesis and immune cell trafficking (52). Western blot analysis showed abundant Gal-1 protein in HDLECs, comparable to its abundance in HMBECs (Fig. 7A). Silencing of *LGALS1* efficiently reduced Gal-1 protein in HDLECs (Fig. 7, B and C), and significantly impaired HDLEC migration in the scratch wound assay (fig. S8A), recapitulating the migration phenotype observed in the screens. Further, silencing of

*LGALS1* in a collagen overlay tube formation assay demonstrated that Gal-1 was also required for proper HDLEC tubule remodelling (Fig. 7D, fig. S8B). *LGALS1* knockdown led to significantly reduced tubule area and thickness, and qualitative failure to establish a network. In an alternative tubule formation assay, Gal-1 knockdown also reduced average tubule length, size, total junctions and total tubule length of HDLECs cocultured with fibroblasts (Fig. 7 E to G and fig. S8C). Similarly knockdown of MICAL2, but not the related MICAL1 (fig. S9C), impaired LEC scratch wound healing (fig. S9, A, B and F) and tubule formation (fig. S9 D to E and G to H), without affecting monolayer integrity or pan-endothelial identity as determined by VE-cadherin at intercellular junctions (fig. S9F). These findings are consistent with the roles of MICAL family proteins in migration and morphogenesis through depolymerisation of actin (*53*). Together, these results provide further evidence that both MICAL2 and Gal-1 promote LEC migration and vessel assembly.

An important aim of this study was to identify potential targets for therapeutic control of pathological lymphangiogenesis and lymphatic remodelling. Gal-1 mediates resistance to VEGFA-targeted anti-angiogenic cancer therapies, related to its promotion of BEC migration by potentiating VEGFA signaling through NRP1 and VEGFR2 (54, 55). It also regulates cell-cell and cell-matrix interactions more broadly, and hence is furthermore implicated in cancer metastasis and immune cell trafficking (52, 56). Indeed, targeting of Gal-1 using inhibitory antibodies or the Gal-1-directed inhibitory peptide Anginex can reduce VEGFA-dependent angiogenesis and tumour growth, as well as altering recruitment of certain leukocyte subsets (55, 57, 58). Thus, targeting Gal-1 in cancer could potentially restrict multiple aspects of tumour progression, including

lymphangiogenesis which is associated with metastasis, and angiogenesis that promotes tumour growth. As further evidence for its role in pathological lymphangiogenesis, Lgals1 mRNA is increased up to 5-fold (unlike Mical2 mRNA, which was decreased) in LECs from inflamed compared to normal ears in the independent CHS microarray dataset (unadjusted p value = 0.0123) (46).

To validate whether Gal-1 also regulated lymphatic vessel remodelling in vivo, we injected mouse ear skin with Gal-1 protein. Ears injected with Gal-1 exhibited both a significantly increased lymphatic vessel density and a 30% increase in vessel width compared to control (Fig. 7H). This increase was abrogated by the addition of the Gal-1-inhibitory peptide Anginex (Fig. 7H). In confirmation, an in vitro assay of lymphangiogenic sprouting from explants of thoracic duct (the major lymphatic trunk) revealed enhancement of lymphangiogenic sprouting by exogenous Gal-1 protein and inhibition of VEGFA-induced lymphangiogenesis by Anginex (fig. S8, D and E). Gal-1 also promoted an increase in CD146-positive blood vessel density in our mouse ear skin model (fig. S10A; Fig. 7H). In an aortic ring explant assay, Anginex inhibited VEGFA-induced angiogenic (BEC) sprouting, although promotion of sprouting by Gal-1 did not reach statistical significance (fig. S10, B and C). Overall, our data suggest that targeting Gal-1 may also be effective at inhibiting tumour-associated lymphangiogenesis or lymphatic remodelling.

In human LN tissue, immunohistochemistry showed that Gal-1 was localized to the endothelium of lymphatic vessels as defined by co-staining with Podoplanin (Fig. 7I). This distribution pattern also validated the detection of *Lgals1* mRNA by microarray in the Podoplanin<sup>+</sup>CD31<sup>+</sup> LECs isolated from mouse LNs, as well as in purified LN BECs

and FRCs (Data File S7). Furthermore, bioinformatic data-mining of the Oncomine<sup>™</sup> database revealed a significant increase in *LGALS1* mRNA expression in tumour stroma from patients with invasive breast cancer (Fig. 7J). Collectively our data point to a role for Gal-1 in promoting lymphangiogenesis and lymphatic remodelling, with potential clinical implications.

Based on the potentiation of VEGFR2 signalling by Gal-1 in BECs (55, 59), we next examined whether Gal-1 depletion influenced HDLEC responses to VEGFA. Compared to control-transfected LECs, HDLECs transfected with *LGALS1* siRNA exhibited enhanced VEGFR2 phosphorylation at Tyr<sup>1175</sup> (required for downstream MAPK signalling (60)) when stimulated with VEGFA, along with significant increases in phosphorylated ERK2 and AKT (Fig. 8, A and B). Phosphorylation of Src family kinases after VEGFA stimulation was slightly but not significantly increased in Gal-1-depleted HDLECs (Fig. 8A; fig. S11, A and B). Gal-1 abundance in *LGALS1*-depleted and Control HDLECs remained relatively constant over the timecourse (fig. S11C). Whilst VEGFC, but not VEGFA, induced phosphorylation of VEGFR3 as expected (fig. S11D), total VEGFR3 abundance was decreased in Gal-1-depleted HDLECs, irrespective of VEGFA stimulation (Fig. 8C). Because VEGFR3 abundance is decreased in BECs postnatally, but maintained at high amounts in LECs (61) (fig. S11E), this result suggested a switch toward a BEC phenotype.

To explore this notion further, we next assessed *LGALS1* siRNA-targeted HDLECs for mRNA and protein of typical LEC- and BEC- selective markers (Fig. 8, D to G; fig. S11F). Knockdown of *LGALS1* was associated with reduced CEACAM1 immunofluorescence and loss of cells with high LYVE1 immunofluorescence (these

being LEC markers), whereas the immunofluorescent signal for the VEGFR2 coreceptor CD146, which is more abundant in BECs than LECs (fig. S11E) (62, 63) was increased (Fig. 8D, fig. S12A). qRTPCR analysis confirmed significantly reduced expression of LYVE1 and increased expression of CD146 mRNA in LGALS1-depleted compared to control-transfected HDLECs (fig. S11F). This analysis also revealed a general trend towards decreased expression of mRNA encoding LEC markers (such as PROX1 and ITGA9) and increased expression of genes typically more abundantly expressed in BECs than LECs (such as TEK, which encodes TIE2, and CD146). This pattern was confirmed by Western blot analyses, which showed that compared to control-transfected HDLECs, LGALS1-depleted HDLECs exhibited significantly decreased abundance of LECcharacteristic proteins VEGFR3, CEACAM1, Podoplanin and the central LEC identity regulator Prox1 (Fig. 8, E to G). In contrast, CD146 and VEGFR2, which are typically more abundant in BECs than LECs (Fig. S11E), were increased (Fig. 8, E to G). Notably, LGALS1 siRNA induced a greater increase in CD146 protein than did siRNAs targeting SOX18 and CEACAM-1, both of which can induce LEC identity in ECs (Fig. 8, E to G; fig. S12, B and C) (64, 65). Given that lower abundance of Prox1, LYVE1, ITGA9 and VEGFR3 compared to initial (microvascular) lymphatics is also characteristic of large collecting lymphatic vessels (66), LGALS1 knockdown could possibly have induced HDLEC differentiation towards a collecting LEC phenotype, although high CD146 abundance has not apparently been reported in collecting lymphatic endothelium. Interrogation of our microarray analysis of collecting vessel LECs (67) suggested that Cd146 was expressed at very low abundance in these cells (fig. S11G). Furthermore, LGALS1 depletion in HDLECs reduced the abundance of Podoplanin (encoded by PDPN

in humans and *Pdpn* in mice), a LEC marker expressed robustly in collecting lymphatic endothelium (fig. S11G) (67). Our data therefore suggest that loss of endogenous *LGALS1* expression induces differentiation of HDLECs towards a blood vascular phenotype. *LGALS1* siRNA-treated HDLECs also maintained CDH5 (VE-cadherin) cell-cell contacts at the wound border that were typically diminished during migration in control-treated HDLECs (Fig. S13A). This corroborated the inhibitory effect of Gal-1 on migration and confirmed, alongside CD31 staining, that endothelial cell identity was maintained (fig. S13, A to B). Together, our results indicate that Gal-1 not only promotes HDLEC migration and remodelling, and modifies VEGFR2 signalling, but also contributes to the maintenance of the lymphatic endothelial phenotype.

## **Discussion**

EC migration is a critical component of sprouting vessel growth and vessel remodelling during development and disease. The scratch wound assay provides a tractable and relevant in vitro model of angiogenesis, as it can replicate both "pioneer" and "follower" modes of migration (13), with potential analogy to "tip" cells and "stalk cells" in three-dimensional angiogenesis (9). Previous siRNA and shRNA screens for regulators of migration in epithelial and endothelial cells cover only a subset of the genome (11-13), while one screen in a fibroblast cell line has interrogated the full genome (68). Our whole-genome approach has revealed multiple signalling pathways and individual genes that control collective migration in a specialized primary human lymphatic EC, the HDLEC.

Of the 154 highly-validated candidate migration genes a proportion have well-

characterised roles in migration across various cell lineages, such as the small GTPase-encoding *CDC42* (69). Further confirmation of the effectiveness of the screen was the high confidence validation of genes with known roles in LEC biology, such as *ANGPT2*, which encodes a ligand for the TIE2 (TEK) receptor. In mice lacking *Angpt2*, lymphatic filopodial sprouting is impaired, and the primary lymphatic plexus fails to remodel into the mature lymphatic hierarchy (25, 31). Furthermore, ANGPT2 promotes tumour lymphangiogenesis (70, 71). *Angpt2* expression was selectively increased in LN LECs during viral-induced remodelling (Data File S7), indicating that it may promote lymphangiogenesis in multiple adult pathological settings.

The biological validity of our siRNA screen was also confirmed by substantial global overlap of our candidate genes with those identified by differential expression in microarray analysis of viral-induced or CHS-associated lymphatic remodelling (Fig. 6). The identification of overlapping genes across differences in species, biological and experimental context, measurement methodology and timeframe gives confidence to their biological relevance in LECs. Genes that were highly validated in the siRNA screens but not detected as differentially expressed in the in vivo models may represent those that are functionally important but are expressed in constant amounts during LEC migration and remodelling. Furthermore, our in vitro migration screen provided evidence of specific gene function that the in vivo microarray analysis alone could not. Notwithstanding that many genes are multifunctional, our screen enabled distinction of siRNA targets that primarily influence proliferation or survival from those chiefly regulating migration. Other siRNA screens using the scratch wound migration assay confirm that cell proliferation does not contribute substantively to wound closure (12, 13). Together, these

analyses suggest that our screening approach identified genes that are relevant to pathological lymphangiogenesis that can be further investigated.

Our siRNA screen uncovered both common and distinct gene functions in LECs and BECs, including some genes that are considered important central regulators of cell migration. Targeting of CDC42 and LIMK1 impaired HDLEC migration, but only mildly inhibited HMBEC migration. Similarly, silencing of CDC42 caused morphological changes in HDLECs that were not seen in HMBECs. This suggests that Rho family GTPases (and their downstream effectors) are differentially regulated in these two related cell types, possibly by the adaptor molecule Afadin (72). Knockdown of certain key migration genes such as WASF2 and PTK2 in HDLECs resulted in lowered cell count, obscuring an observable migration effect. That RHOA and RAC1 were not identified in this screen may reflect insufficient gene silencing or functional depletion; however, it is also possible that these genes may be redundant and therefore not functionally required for migration in HDLECs. For example, RHOC expression was selectively increased in remodelling LN LECs (Data File S7) and its knockdown generated moderate inhibition of migration in the primary screen. Notably, a considerable subset of the candidate genes identified have not previously been associated with cell migration, thus representing an untapped resource for future studies to identify new gene functions. siRNA targeting of several genes (KANSL1, USP25, UGT1A7 and C7orf55) reduced the cell density of HMBECs but not HDLECs. These differences may be critical in optimizing the therapeutic targeting of either, or both, EC types. Indeed, genes classified in our screens as "Low Cell Count" may represent important regulators of survival, proliferation and adhesion. Understanding signalling pathways that trigger EC death may

be important for chemotherapy or radiation therapy in the context of cancer, and as such warrants further investigation.

A goal of this siRNA screen was to identify new therapeutic targets for controlling pathological lymphangiogenesis. To this end, we demonstrated that LGALS1 and MICAL2 are required for HDLEC migration and tube formation. We further confirmed the importance of Gal-1 in supporting LEC migration, remodelling and in vivo lymphangiogenesis. Gal-1 also has an immunological function in the lymphatics in preferentially inhibiting the transmigration of immunogenic rather than tolerogenic dendritic cells into lymphatic vessels (56). A related molecule, Galectin-8, promotes VEGFC-induced lymphatic sprouting and pathological corneal lymphangiogenesis (73, 74). This effect is independent of VEGFR3 and is mediated instead by Podoplanin and α1β1 and α5β1 integrins, in spite of direct interaction of Galectin-8 with VEGFR3. In contrast, Gal-1 does not potentiate VEGFC-induced sprouting (73). In our study Gal-1 promoted VEGFA-induced lymphangiogenesis and lymphatic remodelling through VEGFR2. In BECs, Gal-1 promotes VEGFR2-mediated pro-angiogenic signalling by binding to specific branched N-glycans on VEGFR2 and/or its coreceptors NRP1 (54) and CD146 (59, 75-77). Dimeric Gal-1 can effectively cross-link the receptor complex, thereby inducing VEGF-independent signalling and also increasing retention of receptors on the cell surface, thus prolonging VEGFA-induced signaling (55). Accordingly, we showed that inhibition of Gal-1 activity by siRNA or Anginex impaired lymphangiogenesis (Fig. 7; fig. S8). Possible mechanisms of this effect include interfering with Gal-1-mediated potentiation and prolongation of VEGFR2 signaling and/or blocking Gal-1-mediated interactions with the extracellular matrix (54). Anginex

also binds to Galectins -2, -7, -8N and -9N (78). The role of Gal-1 in promoting lymphangiogenesis was evident in models of Gal-1-mediated lympangiogenic sprouting (thoracic duct explants) and in circumferential expansion of lymphatic vessels (mouse ear model), both of which may involve some LEC proliferation as well as migration given the importance of VEGFR2 signalling in both these processes (18, 79). Whilst CD146 and NRP1 have been implicated in Gal-1's pro-angiogenic activity in BECs, these receptors are typically much less abundant in LECs (62), which suggests that Gal-1's activity on LECs may be predominately mediated through its interaction with VEGFR2, and/or through an alternate receptor yet to be defined. Candidate coreceptors in LECs might include NRP2, or integrins such as  $\alpha 1\beta 1$  which are required for VEGFA-induced LEC migration (79).

While exploring the role of Gal-1 in LEC responses to VEGFA signalling we observed that *LGALS1*-depleted HDLECs had increased protein abundance of VEGFR2 and its coreceptor CD146. The HDLECs apparently were concomitantly sensitised to VEGFA signalling through VEGFR2, showing enhanced phosphorylation of the receptor and its downstream signalling effectors ERK2 and AKT at 10 minutes after addition of VEGFA (Fig. 8, A to B). This enhanced VEGFR2 signaling in *LGALS1*-depleted HDLECs may be a consequence of increased VEGFR2 and CD146 protein abundance. However, the absence of Gal-1's crosslinking effect could also accelerate VEGFR2 internalisation and subsequent degradation upon VEGFA stimulation, leading to an amplified but shorter-lived burst of VEGFR2-initiated signaling from endosomes (55, 60). Depletion or blockade of Gal-1 sensitises resistant tumours to VEGFA-blocking antiangiogenic therapy (55), likely by preventing the VEGFA-independent VEGFR2 signaling induced

by Gal-1-mediated receptor crosslinking, thus restoring VEGFA dependency in tumour ECs. Our data therefore indicate that Gal-1 could similarly influence the sensitivity of tumour lymphatics to VEGFA.

Increased VEGFR2 abundance following LGALS1 knockdown in our HDLECs also appeared to be part of a broader alteration in LEC phenotype (Fig. 8). LGALS1 depletion decreased protein abundance (albeit modestly) of the master LEC identity regulator PROX1, of which a certain threshold amount is required to maintain LEC identity (80, 81). Future studies will determine whether Gal-1 contributes to LEC specification during development, or in the phenotypic plasticity observed in some pathologies (82, 83). Given the association of Gal-1 with VEGFR2, it is possible that Gal-1 sustains LEC phenotype by regulating the balance between endogenous VEGFR2 and VEGFR3mediated signalling. VEGFC signaling through VEGFR3 engages in a positive feedback loop with *PROX1* expression during mouse development and in cultured HDLECs (84), implicating this axis in LEC migration, proliferation and identity. Gal-1 stimulation can induce VEGFR3 phosphorylation in trophoblasts (85), but apparently not in HUVECs (54), which may be due to differences in receptor glycosylation (55). A tentative link between Gal-1 and LEC identity is also suggested by the reprogramming of BECs towards a lymphatic phenotype by Kaposi's Sarcoma Herpesvirus (KSHV) infection (86, 87), and the high abundance of Gal-1 in KS-infected cells (58). Alternatively, intracellular, glycan-independent functions of Gal-1 in Ras localisation or pre-mRNA processing could also be involved in this phenotypic change (88), invoking pathways potentially independent of the VEGFC/VEGFR3/Prox1 axis. CD146 could also be involved in the LEC phenotypic change; depletion of Gal-1 may remove an inhibitory

autocrine feedback loop resulting in increased CD146 abundance. However, several of the Gal-1 receptors present on BECs - CD146, NRP1, integrin  $\alpha1\beta5$  and VEGFR2 – are less abundant or absent on LECs, with some suppressed by PROX1 (89, 90). Therefore, while Gal-1 may have common functions in LECs and BECs with regard to endothelial migration and vessel formation, our data suggest that it may signal in LECs through other pathways that remain to be elucidated.

Our findings, including the identification of several genes not previously implicated in migration and of cell type-specific effects of gene knockdown, elucidate future avenues for research into the biology of lymphatic endothelial cell signalling and antilymphangiogenic therapeutic targeting. We also characterised Gal-1 as a positive regulator of LEC migration and lymphangiogenesis. Together with Gal-1's roles in promoting tumour angiogenesis and its implication in promoting a tolerogenic immune environment (52, 56), our data therefore present a rationale for targeting Gal-1 to inhibit both angiogenesis and lymphangiogenesis in cancer and to enhance anti-tumour immunity.

# **Materials and Methods**

### Cell culture

HDLECs (#CC2812, Lonza) and HMBECs (#CC2813, Lonza) were cultured in endothelial basal medium (EBM)-2 media supplemented with endothelial growth medium (EGM)-2-MV Singlequots (Lonza) and 10 mM 4-(2-Hydroxyethyl)piperazine-1-ethanesulfonic acid (HEPES; Life Technologies). These cells were from a single donor and guaranteed free of pathogens and contaminants by the manufacturer. Tissue culture

treated plates were coated before use with 5  $\mu$ g/ml human fibronectin solution (BD Bioscience). Cells were used at passage number 5. Primary human dermal fibroblasts isolated from foreskins, kindly provided by Dr. Pritinder Kaur (Peter MacCallum Cancer Centre), were grown in DMEM supplemented with 10% fetal calf serum (FCS; v/v), non-essential amino acids, 10 mM HEPES and penicillin-streptomycin (Life Technologies).

### siRNA screen and scratch wound assay.

Detailed Minimum Information About an RNAi Experiment (MIARE)-compliant screening procedures are outlined in Data File S1, and complete protocols are described elsewhere (20). The genome-wide siRNA screen is performed in 96 well plates in technical duplicate (Corning Costar). HDLECs (15000/well) are reverse transfected using DharmaFECT transfection reagent #1 (0.2 µl/well) with 40 nM siRNA (Human siGENOME SMARTpool library [2009 ed.], Dharmacon RNAi Technologies). siRNA pools targeting CDC42 and CDH5 were included as positive controls (fig. S1, D to F). At 48 h post-transfection cells are loaded with Celltracker Green 5-chloromethylfluorescein diacetate (CMFDA) live cell stain (5 µM; Life Technologies) before a 96-pin wounding device with 'FP' pins (V&P Scientific) controlled using a workstation robot (Sciclone ALH 3000, Caliper Life Sciences) is used to create uniform scratches (approximately 3.8 mm long × 0.38 mm wide) in the cell monolayer (fig. S2, A to F). Cells are washed, and medium replaced. An image of the initial scratch area  $(A_0)$  is then obtained as described in High content, high throughput imaging, before incubating at 37°C for a further 24 h. This timepoint represents ~50% closure of the original wound area (fig. S1 E; fig. S3), and is selected to enable detection of both accelerated and inhibited wound closure. At

the assay endpoint, cells are fixed with 4% paraformaldehyde (PFA), then permeabilised and blocked in 0.2% Triton X-100/2% bovine serum albumin (BSA) in phosphatebuffered saline (PBS) and stained with phalloidin CF488 (20 nM, Biotium) and Hoechst 33342 (2  $\mu$ g/ml, Life Technologies). An image of the remaining scratch area (A<sub>24</sub>) is obtained. The area migrated over by the cells in each well is then calculated as  $A_{\rm m} = A_0$  – A<sub>24</sub> (fig. S2, E to F). These values are normalised to the median of mock-transfected wells per plate and averaged across technical replicates. Robust z scores are then generated across all plates (utilizing the median and median absolute deviation; MAD). The "Low Cell Count" threshold is set at < 60% of the median density per field. A curated list of 500 candidates identified in the primary screen is then assayed in a secondary deconvolution screen, with SMARTpool siRNA duplexes assayed individually. The gene list comprises 350 "Impaired" (robust z score <-2.3) and 50 "Accelerated" candidates (robust z score >2.67). In addition, 65 candidate genes (|robust z score| >2) are selected based on known protein-protein interactions with other candidate genes, as these could assist in generating and understanding signalling networks. A further 12 candidates (|robust z score| >2) are selected based on microarray data indicating higher differential expression in HDLECs compared to HMBECs (see Microarray comparison of HDLECs and HMBECs) as these may represent lymphaticspecific migration genes. The list is then rounded to 500 candidates (401 "Impaired" and 99 "Accelerated") by including the candidates with the next highest robust z scores. Transfection follows the protocol of the primary screen, with final siRNA concentration of 25 nM. Thresholds based on mean  $\pm$  3 SD of mock-transfected wells are set at 60% and 130% of mock-transfected cell migration for "Impaired" and "Accelerated" binning

respectively. A gene candidate is deemed validated (here "highly-validated") if two or more of the four siRNA duplexes reproduced the original phenotype seen in the primary screen.

In the tertiary screen, siRNA SMARTpools targeting the 154 "highly-validated" genes identified from the secondary screen are transfected into HDLECs and HMBECs in parallel, following the protocol of the primary screen. The endpoint of the migration assay for HMBECs, at which control scratch wounds were ~50% closed, was experimentally defined as 16 h post-scratch (fig. S6B). The screen is performed in biological duplicate for each cell type, with technical duplicate plates. At the endpoint, cells are additionally stained with Phalloidin CF555 (Biotium).

Official Entrez Gene IDs and gene symbols are from the Human Genome Organisation (HUGO) Gene Nomenclature Committee website (<a href="www.genenames.org">www.genenames.org</a>). Custom python or R scripts are used to quality control, analyse and decipher the siRNA datasets.

### High content, high throughput imaging

Imaging and image processing is performed as described previously (20). Image fields are captured using a high-throughput imaging system (Pathway 435, BD Bioscience), stitched together on capture using acquisition software (Attovision v1.6.1, Becton Dickinson), then smoothed and flattened using image analysis software (MetaMorph v7.7.5.0 (64-bit), Molecular Devices). A fluorescence intensity threshold based on the CellTracker Green and phalloidin CF488 signal is then used to create a binary mask, which enables measurement of the wound area devoid of cells (Fig. S2 E to F). For counting of cell nuclei, a high-content imaging platform (Cellomics VTI Arrayscan,

Thermo Fisher Scientific) is used to acquire 30 adjacent fields per well of cells stained with Hoechst 33342. Thresholding of images is used to identify and count the number of cell nuclei per field.

For cell morphology analysis, cells are additionally stained with Phalloidin CF555 to discriminate filamentous actin. Images are segmented into nuclei and cell body areas using MetaMorph. Segmented areas are then subjected to measurement of various parameters describing cell size and shape, and actin staining intensity as enabled by the Integrated Morphometric Analysis module in MetaMorph (see parameters listed in Fig. 3B). Data for each parameter are normalized into z-scores, and the combined dataset of morphological parameters is then used to determine "clusters" of siRNA target genes whose knockdown generated similar morphologies, as described (20). Briefly, the normalized morphology dataset is subjected to unsupervised hierarchical clustering in CIMminer (http://discover.nci.nih.gov.cimminer/) using Complete linkage cluster method, Correlation distance algorithm and Quantile binning settings. The resulting dendrogram of relatedness (correlation) between genes according to their corresponding morphology parameters is divided into six clusters, guided by a 1-Pearson correlation cutoff of 1.5.

### Antibodies

Antibodies used for immunofluorescence microscopy and Western Blotting were rabbit polyclonal antibodies against human LYVE1 (Fitzgerald RDI), PROX1 (Covance), CEACAM-1 (Abcam) and vWF (DAKO); mouse monoclonal antibodies against human VEGFR3 (clone #54703; R&D Systems), α-smooth muscle actin (α-SMA; clone #1A4,

Sigma), CD146 (clone #P1H12 or SHM-57; BioLegend), CD31 (clone #MEC13.3) PNAd (clone #MECA-79, BD Pharmingen) and CDH5 (VE-cadherin; clone #55-7H1, BD Pharmingen). Rabbit polyclonal antibodies to human Podoplanin (Fitzgerald RDI) and mouse monoclonal antibodies to human CDH2 (clone #5C8, Sigma-Aldrich) and PLVAP (clone #174/2, Hycult Biotech) were used for flow cytometry. A goat polyclonal antibody recognising human Galectin-1 (R&D Systems) and mouse monoclonal antibody to Podoplanin (clone #D2-40; Genway) were used for immunohistochemistry. For Western Blotting, rabbit antibodies against phosphorylated VEGFR2 (Tyr<sup>1175</sup>, clone #19A10), total VEGFR2 (clone #55B11), phosphorylated ERK1/2 (Thr<sup>202</sup>/Tyr<sup>204</sup>), total ERK2, phosphorylated AKT (Ser<sup>473</sup>, clone #D9E), phosphorylated Src family kinases (Tyr<sup>416</sup>, clone #D49G4) and CDC42 (clone #11A11), as well as mouse antibodies to total Akt (clone #40D4) and total Src family kinases (clone #L4A1) were all obtained from Cell Signaling Technology. A mouse monoclonal antibody to human α-tubulin (clone #DM1A; Abcam) or rabbit antibodies to human GAPDH (clone #14C10, Cell Signaling Technology or FL-335, Santa Cruz) were used for loading controls. Isotype control antibodies used for various experiments were mouse IgG1 (BioLegend), rabbit IgG (Imgenex) and goat IgG (Genetex). For immunofluorescence and flow cytometry, goat antibodies recognizing rabbit or mouse IgG and conjugated to Alexa Fluor 488 or 546 were used. For Western blotting, secondary antibodies recognising goat, mouse or rabbit IgG conjugated to IRdye 800 or IRdye 680 (LI-COR) were used.

# Signaling pathway analysis

Pathway analysis software (Metacore, GeneGo, Thompson Reuters) was used to search

for signaling pathways ("Pathway Maps") and cellular processes ("GO Processes") that were overrepresented in the datasets. Input datasets are compared to lists of genes within the database that are annotated to particular terms (such as a given "Pathway Map"). *P* values calculated in enrichment analyses indicate the probability that the number of genes represented in both the input dataset and the annotated term list is random, and are derived according to hypergeometric distributions.

The software also allowed construction of protein–protein interaction networks using various algorithms as follows. A "direct interactions" or a "shortest paths" algorithm (maximum number of steps = 2, not canonical pathways) was used for generating signaling networks (Fig. 5). Networks were constructed to identify protein-protein interactions using direct interaction types (such as phosphorylation, binding, cleavage), however, indirect interactions ("transcriptional regulation" and "influence on expression") were excluded. Open-source software (Cytoscape v.2.8.2; www.cytoscape.org) was employed for visualizing and integrating data into networks, following data importation from Metacore using the plugin "com.genego.cytplugin.NetworkLoader" (v.0.1). Construction of an ontology tree was performed using GOrilla (<a href="http://cbl-gorilla.cs.technion.ac.il/">http://cbl-gorilla.cs.technion.ac.il/</a>), which enabled comparison of the candidate gene list with the rest of the human genome.

Isolation of LN stromal and endothelial cells in a cutaneous HSV-1 infection model.

All animal experiments were conducted under the approval of the Animal Experimental

Ethics Committees at Peter MacCallum Cancer Centre or the Peter Doherty Institute.

Detailed protocols for LN stromal cell subset isolation and microarray analysis (see

below) are described elsewhere (*45*, *91*). Briefly, C57Bl/6 mice are inoculated with HSV-1 onto a patch of abraded skin. Brachial LNs draining the infection site are harvested from uninfected mice or on day 6 after inoculation and digested to a single-cell suspension for flow cytometric cell sorting. After gating out residual CD45<sup>+</sup> leukocytes, LECs are defined as Podoplanin<sup>+</sup>CD31<sup>+</sup>, BECs as Podoplanin<sup>-</sup>CD31<sup>+</sup>, and FRCs as Podoplanin<sup>1</sup>owCD31<sup>-</sup>.

#### Microarray analysis of LN stromal cell subsets and list overlap analysis.

Biotinylated cDNA derived from sorted LN cell subsets is hybridized to GeneChip MouseGene 1.0 ST chips (Affymetrix). After processing and normalization of microarray probe intensity data using robust multi-array analysis (RMA) (92), differential expression is analyzed using the limma software package (93) in BioConductor (94). TREAT (T-tests RElative to A Threshold) empirical Bayes t-tests (95) relative to a fold change threshold of 1.1 are applied to determine significance of differential expression, with the false discovery rate (FDR) set at 5%. This dataset is published (45) and deposited in the Gene Expression Omnibus (GEO) database (www.ncbi.nlm.nih.gov/geo; GSE84284). The same analysis was also applied to a publicly-available microarray dataset comprising LECs isolated from untreated and CHS-inflamed mouse ears (46). The matrix file containing RMA-normalised data from the GeneChip Mouse Genome 430 2.0 Array (Affymetrix) was downloaded from GEO (accession number GSE26229), and differential expression analysed using limma with TREAT criteria as above. In the case of multiple probes per gene, a single representative probe was chosen.

For the comparison between the microarray datasets and siRNA screen results, we applied a further threshold of |linear fold-change| ≥1.8 on top of the 5% false discovery rate (FDR; P < 0.05 after adjustment for multiple testing) to increase stringency on the biological significance of changes in mRNA expression. For the LN stromal cell dataset, lists of genes that were selectively differentially-expressed by the three cell types (BEC, LEC or FRC) were also derived as described in Fig. 6D to interrogate shared and cell type-selective effects. Differentially-expressed genes were considered to be "-selective" to the designated cell type or types in this experimental context if they were either not differentially expressed (i.e. |fold-change|<1.8), or discordantly differentially expressed (i.e. |fold-change|≥1.8 in the opposite direction) in the other cell types. For the CHS dataset (46), only one cell type had been analysed so all genes differentially-expressed with |linear fold change|  $\geq 1.8$  and adjusted P > 0.05 were included, analogous to the LEC total list from the LN stromal cell dataset (Fig. 6D). Mouse gene symbols from microarray data were converted to human orthologs using the HUGO Gene Nomenclature Committee Comparison of Orthology Predictions (HCOP) retrieved from http://www.genenames.org/cgi-bin/hcop, selecting the ortholog predicted by the greatest number of databases. Sorted lists of differentially-expressed genes from the microarray datasets were then compared with genes identified from the siRNA screen experiments to derive lists of overlapping genes. Data presented are derived from pooled lists of all increased and decreased differentially-expressed genes fitting the above criteria compared to "Accelerated" and "Impaired" "expanded migration candidates" with robust z score ≥1.6449 in the primary siRNA screen, representing the top 5% and bottom 5% of scores.

Genes binned as "Low Cell Count" in the primary screen were excluded prior to overlap analysis.

Statistical significance of overlap was determined empirically using simulated null distributions, a useful strategy for comparing similarity of gene lists from different sources (96). These were derived by determining the overlap between 10,000 pairs of random gene lists of the same size as derived by the criteria above, relative to the complete list for each different analysis platform (18,120 human genes for the Human siGENOME SMARTpool library; 21,041 mouse genes for the GeneChip MouseGene 1.0 ST microarray; 21,723 genes for the GeneChip Mouse Genome 430 2.0 Array). Genes were indexed as integers and randomly sampled without replacement, assuming that the mouse microarray probes have one-to-one mapping to human siRNA targets and that the genes covered by the microarray are a superset of the genes targeted in the siRNA library. The size of the lists of overlapping genes was then assessed for significance against the null distribution. Analyses were performed using R statistical software. As a further validation, significance was also computed based on hypergeometric distribution over the common set of genes between the two platforms. Hypergeometric P values correlated with empirical P values calculated from simulated null distributions, and gave a more conservative estimate of significance.

### Tube formation and co-culture assays

HDLECs were reverse transfected with gene-targeting siRNA SMARTpools or a control siRNA (ON-TARGETplus Non-targeting control pool, Dharmacon). For short-term overlay tube formation assays, 48 h post-transfection the cells were overlaid with  $100~\mu l$ 

neutralized collagen solution (Bovine Type 1, Gibco) and incubated at 37°C, 5% CO<sub>2</sub> for 8 h to allow tube formation to occur (97). Collagen overlaid cells were fixed in 4% PFA and permeabilized with 0.2% Triton-X 100, 1% BSA in PBS. Cells were washed with PBS and stained with phalloidin CF488 (20 nM, Biotium) and Hoechst 33342. Images were captured (Cellomics VTI Arrayscan, Thermo Fisher Scientific) using a 5× Fluar NA0.25 objective (Carl Zeiss), with 9 adjacent fields imaged per well. Images were autocontrast adjusted using Adobe Photoshop CS4 (Adobe Systems Incorporated), and quantified using a custom analysis protocol established in image analysis software (MetaMorph). The co-culture assays were performed as described previously (98) with the following modifications. Briefly, 10<sup>4</sup> primary dermal fibroblasts per well were grown in 96 well plates. 24 h after siRNA treatment, HDLECs were seeded at 1.5x10<sup>3</sup> cells per well onto the fibroblast feeder layer and grown for nine days before fixation and processing for immunofluorescence microscopy. Tubule formation was analysed using either ImageJ or Angioquant (http://www.cs.tut.fi/sgn/csb/angioquant/) programs.

#### SDS-PAGE and Western blotting

Protein abundance was assessed using SDS-PAGE and Western blotting as described previously (99). Briefly, for analysis of phosphorylation in VEGFA and VEGFC signaling pathways, siRNA-treated cells were serum-starved in MCDB-131 media (GE, Life Technologies) supplemented with 0.2% BSA for 2-4 h prior to stimulation with recombinant human VEGFA<sub>165</sub> (R&D Systems) or mature VEGFC (Opthea) for indicated times. Cells were washed 3 times in ice-cold PBS prior to lysis in 2% sodium dodecyl sulfate (SDS) Buffer (2% SDS, 50mM Tris, 150mM NaCl, 2mM ethylenediaminetetraacetic acid [EDTA], 2mM ethylene glycol-bis(β-aminoethyl ether)-

N,N,N',N'-tetraacetic acid [EGTA], 1mM phenylmethylsulfonylfluoride) and protein quantification by bicinchoninic acid assay (Pierce). 10-15 µg total protein was separated on 4-20% Bolt gels before transfer using the iBlot system (GE, Life Technologies). Western blotting was performed using primary antibodies as described above and imaged using either Odyssey CLx Imaging System (LI-COR) for infrared fluorescence detection or a GelDoc (BioRad) for chemiluminescence-based development.

# Injection of Matrigel Plugs into Mouse Ears

Recombinant mouse Gal-1, VEGFA, a mature form of mouse VEGFD, Anginex or BSA (Control) were resuspended in 30  $\mu$ l of Matrigel (Matrigel Basement Membrane Matrix, BD Biosciences) at either 10 or 25  $\mu$ g/ml final concentration and injected into the center of 6-8-week old female SCID/NOD (severe combined immunodeficent/nonobese diabetic)/Gamma mouse ears. At 5 days post injection, ears were harvested, fixed and processed for staining of lymphatic (LYVE-1 or Podoplanin) and blood vasculature (CD146 or  $\alpha$ SMA). Images were captured on either Pathway 435 or BX61 (Olympus) microscope and analyzed using Metamorph and AngioTool software.

#### Immunofluorescence staining and quantitation

Cells were treated as for the siRNA screen and scratch wound assay and subsequently stained with appropriate primary and fluorescently-conjugated secondary antibodies. Fluorescence images were captured using the Cellomics VTI Arrayscan or Pathway 435 automated high-throughput microscopy platforms. To quantify immunofluorescence staining for particular antigens, fluorescence intensity was measured using ImageJ following the application of a common threshold across all samples within a single 96-

well plate. A mask was applied based on the highest-expressing sample and pixel intensity determined across the various conditions. Immunofluorescence staining of mouse LN sections is described elsewhere (45).

# **Immunohistochemistry**

Human lymph node tissue sections were obtained from the Molecular Pathology
Department, Peter MacCallum Cancer Centre. Samples were from breast cancer patients with no lymph node metastases. Samples were obtained with informed consent, and used under appropriate institutional approval. Microwave antigen retrieval of paraffin embedded sections was performed using target retrieval solution (DAKO), for 15 min on medium low setting. Endogenous peroxidase was blocked by washing slides in 3% H<sub>2</sub>0<sub>2</sub>/methanol for 20 min, and then adding serum-free blocking solution (DAKO) for 1 h. Sections were immunostained with a goat antibody recognizing human Gal-1 (1:100), or a mouse antibody against Podoplanin (1:100), and an appropriate biotinylated secondary antibody. Signal was amplified using Vectastain ABC (Vector Laboratories), and developed using liquid diaminobenzidine (DAB) (Peroxidase Substrate Kit, Vector Laboratories). Slides were subsequently visualized and imaged using a microscope (BX61, Olympus) with 60× UPlanSApo NA1.20 objective (Olympus) and digital camera (SPOT RT3 Slider, Diagnostic Instruments).

#### qRT-PCR

Total RNA isolated from HDLECs was reverse-transcribed using the High-Capacity cDNA reverse transcription kit (Applied Biosystems) according to the manufacturer's

instructions. Expression of selected genes was then assessed using Taqman gene expression assays and gene expression master mix (Applied Biosystems). Target abundance was normalized to *GAPDH*.

# Oncomine<sup>TM</sup> data analysis

The relative expression of individual candidate migration genes in human breast tumor stroma samples was determined by searching the Oncomine database (version 4.4.3, September 2012 data release, <a href="www.oncomine.org">www.oncomine.org</a>). Target genes (for example *LGALS1*) were queried, and output data was sorted to isolate "cancer versus normal" associations, filtered using the tissue subtype "stroma". Data is reported as the log2 median-centered expression values for normal breast and breast carcinoma samples using box-and-whiskers plots. *LGALS1* expression in normal compared to cancer groups was compared within Oncomine using a two sample t-test.

#### Thoracic Duct and Aortic ring sprouting assay

Thoracic ducts and aortae from male or female 6-12 week-old C57Bl/6 mice were isolated and processed for the assay essentially as outlined by Bruyère et al. (91) or Baker et al. (92) with some modifications. Briefly, small sections of upper thoracic duct or aorta were micro-dissected and embedded in neutralized type I rat tail collagen (1 mg/ml in Opti-MEM [Life Technologies] supplemented with 2% FCS). Explants were grown for 5 days in Opti-MEM supplemented with 10% FCS for thoracic ducts or 2.5% FCS for aortae and either growth factors, recombinant Gal-1 or Anginex. Collagen gels were fixed in 4% PFA, permeabilised with 0.25% Triton-X-100 in PBS, and stained for sprouting

endothelium (*Bandiera* (*Griffonia*) *Simplicifolia* (BS)1-Lectin-FITC) and outgrowing supporting cells (Phalloidin-Alexa Fluor 555). Images were captured on a Pathway 435 and collapsed z-stack images were quantified using ImageJ for endothelial outgrowth area and tubule length. Sprout numbers were manually scored.

#### Microarray comparison of HDLECs and HMBECs

Publicly available microarray dataset GSE6550-GPL570 was accessed through GEO. The GEO2R analysis function on the website was used to analyze the data and calculate the fold change in expression for each gene between blood and lymphatic ECs. The values of multiple probes were averaged, and a mean fold-change of  $\geq 10$  was used to select genes with differential expression.

#### General statistical analysis

For experiments involving comparison of treated and control groups, a two-tailed Student's t-test was used. A one-way analysis of variance (ANOVA) test with Dunnett (comparison to control) or Tukey (comparison to all samples) post-hoc test was used for comparison of multiple groups in various experiments. With the exception of the list overlap analyses, and analyses performed within Metacore and Oncomine, statistical analyses were conducted using Graphpad Prism software (versions 5-7). P < 0.05 was considered statistically significant. The appropriateness of the tests used has been affirmed by Dr. E. Link, a senior statistician at Peter MacCallum Cancer Centre.

# **Supplementary Materials**

- Fig. S1: Optimization of LEC scratch wound migration assay
- Fig. S2: High-throughput scratch wound migration assay
- Fig. S3: Genome-wide siRNA screen assay timing
- Fig. S4: Gene ontology classification of validated regulators of HDLEC migration
- Fig. S5: HDLEC morphology cluster phenotypes and corresponding migration scores
- Fig. S6: BEC migration assay
- Fig. S7: Comparison of selected HMBEC and HDLEC morphology phenotypes
- Fig. S8: Validation of a role for LGALS1 in LEC migration and remodeling
- Fig. S9: Validation of a role for MICAL2 in LEC migration and remodeling
- Fig. S10: Effect of Galectin-1 on angiogenesis and blood vessel remodeling
- Fig. S11: VEGFR signaling and lineage marker abundance in HDLECs
- Fig. S12: Immunofluorescence analysis of CD146 protein in HDLECs
- Fig. S13: Immunofluorescence analysis of LEC and common endothelial marker proteins
- in LGALS1-depleted HDLECs
- Data File S1: MIARE siRNA screen descriptors
- Data File S2: Aggregated siRNA screen and LN microarray results
- Data File S3: Primary Screen Pathway Enrichment Analysis
- Data File S4: Primary Screen Gene Ontology Enrichment Analysis
- Data File S5: Secondary Screen Gene Ontology Enrichment Analysis
- Data File S6: Secondary Screen Pathway Enrichment Analysis
- Data File S7: Overlapping genes detected in LECs in siRNA screen and LN microarray
- Data File S8: Overlapping genes detected in LECs in siRNA screen and dermal CHS

#### **References and Notes**

- 1. K. Alitalo, The lymphatic vasculature in disease. *Nat Med* **17**, 1371-1380 (2011)
- 2. M. A. Swartz, A. W. Lund, Lymphatic and interstitial flow in the tumour microenvironment: linking mechanobiology with immunity. *Nat Rev Cancer* **12**, 210-219 (2012)
- 3. S. Liao, P. Y. von der Weid, Lymphatic system: an active pathway for immune protection. *Semin Cell Dev Biol* **38**, 83-89 (2015)
- 4. S. A. Stacker, S. P. Williams, T. Karnezis, R. Shayan, S. B. Fox, M. G. Achen, Lymphangiogenesis and lymphatic vessel remodelling in cancer. *Nat Rev Cancer* **14**, 159-172 (2014)
- 5. S. Hirakawa, L. F. Brown, S. Kodama, K. Paavonen, K. Alitalo, M. Detmar, VEGF-C-induced lymphangiogenesis in sentinel lymph nodes promotes tumor metastasis to distant sites. *Blood* **109**, 1010-1017 (2007)
- 6. S. A. Stacker, C. Caesar, M. E. Baldwin, G. E. Thornton, R. A. Williams, R. Prevo, D. G. Jackson, S. Nishikawa, H. Kubo, M. G. Achen, VEGF-D promotes the metastatic spread of tumor cells via the lymphatics. *Nat Med* 7, 186-191 (2001)
- 7. G. D'Amico, D. T. Jones, E. Nye, K. Sapienza, A. R. Ramjuan, L. E. Reynolds, S. D. Robinson, V. Kostourou, D. Martinez, D. Aubyn, R. Grose, G. J. Thomas, B. Spencer-Dene, D. Zicha, D. Davies, V. Tybulewicz, K. M. Hodivala-Dilke, Regulation of lymphatic-blood vessel separation by endothelial Rac1. *Development* **136**, 4043-4053 (2009)
- 8. M. Caunt, J. Mak, W. C. Liang, S. Stawicki, Q. Pan, R. K. Tong, J. Kowalski, C. Ho, H. B. Reslan, J. Ross, L. Berry, I. Kasman, C. Zlot, Z. Cheng, J. Le Couter, E. H. Filvaroff, G. Plowman, F. Peale, D. French, R. Carano, A. W. Koch, Y. Wu, R. J. Watts, M. Tessier-Lavigne, A. Bagri, Blocking neuropilin-2 function inhibits tumor cell metastasis. *Cancer Cell* 13, 331-342 (2008)
- 9. P. Rorth, Fellow travellers: emergent properties of collective cell migration. *EMBO Rep* **13**, 984-991 (2012)
- 10. A. Mogilner, K. Keren, The shape of motile cells. *Curr Biol* **19**, R762-771 (2009)
- 11. C. S. Collins, J. Hong, L. Sapinoso, Y. Zhou, Z. Liu, K. Micklash, P. G. Schultz, G. M. Hampton, A small interfering RNA screen for modulators of tumor cell motility identifies MAP4K4 as a promigratory kinase. *Proc Natl Acad Sci U S A* **103**, 3775-3780 (2006)
- 12. K. J. Simpson, L. M. Selfors, J. Bui, A. Reynolds, D. Leake, A. Khvorova, J. S. Brugge, Identification of genes that regulate epithelial cell migration using an siRNA screening approach. *Nat Cell Biol* **10**, 1027-1038 (2008)
- 13. P. Vitorino, T. Meyer, Modular control of endothelial sheet migration. *Genes Dev* **22**, 3268-3281 (2008)
- 14. L. Lamalice, F. Le Boeuf, J. Huot, Endothelial cell migration during angiogenesis. *Circ Res* **100**, 782-794 (2007)
- 15. C. C. Liang, A. Y. Park, J. L. Guan, In vitro scratch assay: a convenient and inexpensive method for analysis of cell migration in vitro. *Nat Protoc* **2**, 329-333 (2007)

- T. Makinen, L. Jussila, T. Veikkola, T. Karpanen, M. I. Kettunen, K. J. Pulkkanen, R. Kauppinen, D. G. Jackson, H. Kubo, S. Nishikawa, S. Yla-Herttuala, K. Alitalo, Inhibition of lymphangiogenesis with resulting lymphedema in transgenic mice expressing soluble VEGF receptor-3. *Nature Med.* 7, 199-205 (2001)
- 17. Y. Xu, L. Yuan, J. Mak, L. Pardanaud, M. Caunt, I. Kasman, B. Larrivee, R. Del Toro, S. Suchting, A. Medvinsky, J. Silva, J. Yang, J. L. Thomas, A. W. Koch, K. Alitalo, A. Eichmann, A. Bagri, Neuropilin-2 mediates VEGF-C-induced lymphatic sprouting together with VEGFR3. *J Cell Biol* 188, 115-130 (2010)
- T. Makinen, T. Veikkola, S. Mustjoki, T. Karpanen, B. Catimel, E. C. Nice, L. Wise, A. Mercer, H. Kowalski, D. Kerjaschki, S. A. Stacker, M. G. Achen, K. Alitalo, Isolated lymphatic endothelial cells transduce growth, survival and migratory signals via the VEGF-C/D receptor VEGFR-3. *The EMBO journal* 20, 4762-4773 (2001)
- N. Davydova, N. C. Harris, S. Roufail, S. Paquet-Fifield, M. Ishaq, V. A. Streltsov, S. P. Williams, T. Karnezis, S. A. Stacker, M. G. Achen, Differential Receptor Binding and Regulatory Mechanisms for the Lymphangiogenic Growth Factors Vascular Endothelial Growth Factor (VEGF)-C and -D. *J Biol Chem* 291, 27265-27278 (2016)
- 20. S. P. Williams, C. M. Gould, C. J. Nowell, T. Karnezis, M. G. Achen, K. J. Simpson, S. A. Stacker, Systematic high-content genome-wide RNAi screens of endothelial cell migration and morphology. *Sci Data* **4**, 170009 (2017)
- A. Birmingham, L. M. Selfors, T. Forster, D. Wrobel, C. J. Kennedy, E. Shanks, J. Santoyo-Lopez, D. J. Dunican, A. Long, D. Kelleher, Q. Smith, R. L. Beijersbergen, P. Ghazal, C. E. Shamu, Statistical methods for analysis of highthroughput RNA interference screens. *Nat Methods* 6, 569-575 (2009)
- 22. N. E. Banziger-Tobler, C. Halin, K. Kajiya, M. Detmar, Growth hormone promotes lymphangiogenesis. *Am J Pathol* **173**, 586-597 (2008)
- 23. A. S. Lee, D. H. Kim, J. E. Lee, Y. J. Jung, K. P. Kang, S. Lee, S. K. Park, J. Y. Kwak, S. Y. Lee, S. T. Lim, M. J. Sung, S. R. Yoon, W. Kim, Erythropoietin induces lymph node lymphangiogenesis and lymph node tumor metastasis. *Cancer Res* **71**, 4506-4517 (2011)
- 24. R. Cao, M. A. Bjorndahl, P. Religa, S. Clasper, S. Garvin, D. Galter, B. Meister, F. Ikomi, K. Tritsaris, S. Dissing, T. Ohhashi, D. G. Jackson, Y. Cao, PDGF-BB induces intratumoral lymphangiogenesis and promotes lymphatic metastasis. *Cancer Cell* **6**, 333-345 (2004)
- N. W. Gale, G. Thurston, S. F. Hackett, R. Renard, Q. Wang, J. McClain, C. Martin, C. Witte, M. H. Witte, D. Jackson, C. Suri, P. A. Campochiaro, S. J. Wiegand, G. D. Yancopoulos, Angiopoietin-2 is required for postnatal angiogenesis and lymphatic patterning, and only the latter role is rescued by angiopoietin-1. *Dev Cell* 3, 411-423 (2002)
- 26. M. J. Schell, C. Erneux, R. F. Irvine, Inositol 1,4,5-trisphosphate 3-kinase A associates with F-actin and dendritic spines via its N terminus. *J Biol Chem* **276**, 37537-37546 (2001)

- 27. M. H. Wu, N. W. Ying, T. M. Hong, W. F. Chiang, Y. T. Lin, Y. L. Chen, Galectin-1 induces vascular permeability through the neuropilin-1/vascular endothelial growth factor receptor-1 complex. *Angiogenesis* 17, 839-849 (2014)
- D. J. de Gorter, E. A. Beuling, R. Kersseboom, S. Middendorp, J. M. van Gils, R. W. Hendriks, S. T. Pals, M. Spaargaren, Bruton's tyrosine kinase and phospholipase Cgamma2 mediate chemokine-controlled B cell migration and homing. *Immunity* 26, 93-104 (2007)
- M. Spaargaren, E. A. Beuling, M. L. Rurup, H. P. Meijer, M. D. Klok, S. Middendorp, R. W. Hendriks, S. T. Pals, The B cell antigen receptor controls integrin activity through Btk and PLCgamma2. *J Exp Med* 198, 1539-1550 (2003)
- 30. S. Sharma, G. Orlowski, W. Song, Btk regulates B cell receptor-mediated antigen processing and presentation by controlling actin cytoskeleton dynamics in B cells. *J Immunol* **182**, 329-339 (2009)
- 31. M. Dellinger, R. Hunter, M. Bernas, N. Gale, G. Yancopoulos, R. Erickson, M. Witte, Defective remodeling and maturation of the lymphatic vasculature in Angiopoietin-2 deficient mice. *Dev Biol* **319**, 309-320 (2008)
- 32. L. Hakanpaa, T. Sipila, V. M. Leppanen, P. Gautam, H. Nurmi, G. Jacquemet, L. Eklund, J. Ivaska, K. Alitalo, P. Saharinen, Endothelial destabilization by angiopoietin-2 via integrin beta1 activation. *Nat Commun* **6**, 5962 (2015)
- 33. Z. Yang, H. Wang, Y. Jiang, M. E. Hartnett, VEGFA activates erythropoietin receptor and enhances VEGFR2-mediated pathological angiogenesis. *Am J Pathol* **184**, 1230-1239 (2014)
- 34. M. Hu, X. J. Sun, Y. L. Zhang, Y. Kuang, C. Q. Hu, W. L. Wu, S. H. Shen, T. T. Du, H. Li, F. He, H. S. Xiao, Z. G. Wang, T. X. Liu, H. Lu, Q. H. Huang, S. J. Chen, Z. Chen, Histone H3 lysine 36 methyltransferase Hypb/Setd2 is required for embryonic vascular remodeling. *Proc Natl Acad Sci U S A* **107**, 2956-2961 (2010)
- 35. J. Dias, N. Van Nguyen, P. Georgiev, A. Gaub, J. Brettschneider, S. Cusack, J. Kadlec, A. Akhtar, Structural analysis of the KANSL1/WDR5/KANSL2 complex reveals that WDR5 is required for efficient assembly and chromatin targeting of the NSL complex. *Genes & development* 28, 929-942 (2014)
- S. Goettsch, W. Goettsch, H. Morawietz, P. Bayer, Shear stress mediates tyrosylprotein sulfotransferase isoform shift in human endothelial cells. *Biochem Biophys Res Commun* 294, 541-546 (2002)
- 37. T. Reid, T. Furuyashiki, T. Ishizaki, G. Watanabe, N. Watanabe, K. Fujisawa, N. Morii, P. Madaule, S. Narumiya, Rhotekin, a new putative target for Rho bearing homology to a serine/threonine kinase, PKN, and rhophilin in the rho-binding domain. *J Biol Chem* **271**, 13556-13560 (1996)
- 38. G. Li, C. Gustafson-Brown, S. K. Hanks, K. Nason, J. M. Arbeit, K. Pogliano, R. M. Wisdom, R. S. Johnson, c-Jun is essential for organization of the epidermal leading edge. *Dev Cell* 4, 865-877 (2003)
- 39. S. Hirakawa, Y. K. Hong, N. Harvey, V. Schacht, K. Matsuda, T. Libermann, M. Detmar, Identification of vascular lineage-specific genes by transcriptional profiling of isolated blood vascular and lymphatic endothelial cells. *Am J Pathol* **162**, 575-586 (2003)

- 40. M. Merkel, R. H. Eckel, I. J. Goldberg, Lipoprotein lipase: genetics, lipid uptake, and regulation. *Journal of lipid research* **43**, 1997-2006 (2002)
- 41. W. Dong, H. Gong, G. Zhang, S. Vuletic, J. Albers, J. Zhang, H. Liang, Y. Sui, J. Zheng, Lipoprotein lipase and phospholipid transfer protein overexpression in human glioma cells and their effect on cell growth, apoptosis, and migration. *Acta Biochim Biophys Sin (Shanghai)* 49, 62-73 (2017)
- 42. M. Fernandez-Borja, D. Bellido, R. Makiya, G. David, G. Olivecrona, M. Reina, S. Vilaro, Actin cytoskeleton of fibroblasts organizes surface proteoglycans that bind basic fibroblast growth factor and lipoprotein lipase. *Cell Motil Cytoskeleton* **30**, 89-107 (1995)
- 43. R. S. Kota, C. V. Ramana, F. A. Tenorio, R. I. Enelow, J. C. Rutledge, Differential effects of lipoprotein lipase on tumor necrosis factor-alpha and interferon-gamma-mediated gene expression in human endothelial cells. *J Biol Chem* 280, 31076-31084 (2005)
- 44. E. M. Hur, F. Q. Zhou, GSK3 signalling in neural development. *Nat Rev Neurosci* 11, 539-551 (2010)
- 45. J. L. Gregory, A. Walter, Y. O. Alexandre, J. L. Hor, R. Liu, J. Z. Ma, S. Devi, N. Tokuda, Y. Owada, L. K. Mackay, G. K. Smyth, W. R. Heath, S. N. Mueller, Infection Programs Sustained Lymphoid Stromal Cell Responses and Shapes Lymph Node Remodeling upon Secondary Challenge. *Cell Rep* 18, 406-418 (2017)
- B. Vigl, D. Aebischer, M. Nitschke, M. Iolyeva, T. Rothlin, O. Antsiferova, C. Halin, Tissue inflammation modulates gene expression of lymphatic endothelial cells and dendritic cell migration in a stimulus-dependent manner. *Blood* 118, 205-215 (2011)
- 47. R. Kunstfeld, S. Hirakawa, Y. K. Hong, V. Schacht, B. Lange-Asschenfeldt, P. Velasco, C. Lin, E. Fiebiger, X. Wei, Y. Wu, D. Hicklin, P. Bohlen, M. Detmar, Induction of cutaneous delayed-type hypersensitivity reactions in VEGF-A transgenic mice results in chronic skin inflammation associated with persistent lymphatic hyperplasia. *Blood* **104**, 1048-1057 (2004)
- 48. W. E. Cromer, S. D. Zawieja, B. Tharakan, E. W. Childs, M. K. Newell, D. C. Zawieja, The effects of inflammatory cytokines on lymphatic endothelial barrier function. *Angiogenesis* **17**, 395-406 (2014)
- 49. G. V. Chaitanya, S. E. Franks, W. Cromer, S. R. Wells, M. Bienkowska, M. H. Jennings, A. Ruddell, T. Ando, Y. Wang, Y. Gu, M. Sapp, J. M. Mathis, P. A. Jordan, A. Minagar, J. S. Alexander, Differential cytokine responses in human and mouse lymphatic endothelial cells to cytokines in vitro. *Lymphat Res Biol* 8, 155-164 (2010)
- 50. C. H. Lin, J. Lu, H. Lee, Interleukin-1beta expression is required for lysophosphatidic Acid-induced lymphangiogenesis in human umbilical vein endothelial cells. *International journal of inflammation* **2011**, 351010 (2010)
- F. Benahmed, S. Chyou, D. Dasoveanu, J. Chen, V. Kumar, Y. Iwakura, T. T. Lu, Multiple CD11c+ cells collaboratively express IL-1beta to modulate stromal vascular endothelial growth factor and lymph node vascular-stromal growth. *J Immunol* 192, 4153-4163 (2014)

- 52. G. A. Rabinovich, J. R. Conejo-Garcia, Shaping the Immune Landscape in Cancer by Galectin-Driven Regulatory Pathways. *J Mol Biol* **428**, 3266-3281 (2016)
- 53. S. S. Giridharan, S. Caplan, MICAL-family proteins: Complex regulators of the actin cytoskeleton. *Antioxid Redox Signal* **20**, 2059-2073 (2014)
- 54. S. H. Hsieh, N. W. Ying, M. H. Wu, W. F. Chiang, C. L. Hsu, T. Y. Wong, Y. T. Jin, T. M. Hong, Y. L. Chen, Galectin-1, a novel ligand of neuropilin-1, activates VEGFR-2 signaling and modulates the migration of vascular endothelial cells. *Oncogene* 27, 3746-3753 (2008)
- D. O. Croci, J. P. Cerliani, T. Dalotto-Moreno, S. P. Mendez-Huergo, I. D. Mascanfroni, S. Dergan-Dylon, M. A. Toscano, J. J. Caramelo, J. J. Garcia-Vallejo, J. Ouyang, E. A. Mesri, M. R. Junttila, C. Bais, M. A. Shipp, M. Salatino, G. A. Rabinovich, Glycosylation-dependent lectin-receptor interactions preserve angiogenesis in anti-VEGF refractory tumors. *Cell* 156, 744-758 (2014)
- 56. S. Thiemann, J. H. Man, M. H. Chang, B. Lee, L. G. Baum, Galectin-1 regulates tissue exit of specific dendritic cell populations. *J Biol Chem* **290**, 22662-22677 (2015)
- V. L. Thijssen, R. Postel, R. J. Brandwijk, R. P. Dings, I. Nesmelova, S. Satijn, N. Verhofstad, Y. Nakabeppu, L. G. Baum, J. Bakkers, K. H. Mayo, F. Poirier, A. W. Griffioen, Galectin-1 is essential in tumor angiogenesis and is a target for antiangiogenesis therapy. *Proc Natl Acad Sci U S A* 103, 15975-15980 (2006)
- D. O. Croci, M. Salatino, N. Rubinstein, J. P. Cerliani, L. E. Cavallin, H. J. Leung, J. Ouyang, J. M. Ilarregui, M. A. Toscano, C. I. Domaica, M. C. Croci, M. A. Shipp, E. A. Mesri, A. Albini, G. A. Rabinovich, Disrupting galectin-1 interactions with N-glycans suppresses hypoxia-driven angiogenesis and tumorigenesis in Kaposi's sarcoma. *J Exp Med* 209, 1985-2000 (2012)
- 59. N. D'Haene, S. Sauvage, C. Maris, I. Adanja, M. Le Mercier, C. Decaestecker, L. Baum, I. Salmon, VEGFR1 and VEGFR2 involvement in extracellular galectin-1-and galectin-3-induced angiogenesis. *PloS one* **8**, e67029 (2013)
- 60. A. Eichmann, M. Simons, VEGF signaling inside vascular endothelial cells and beyond. *Curr Opin Cell Biol* **24**, 188-193 (2012)
- 61. A. Kaipainen, J. Korhonen, T. Mustonen, V. W. van Hinsbergh, G. H. Fang, D. Dumont, M. Breitman, K. Alitalo, Expression of the fms-like tyrosine kinase 4 gene becomes restricted to lymphatic endothelium during development. *Proc.Natl.Acad.Sci. USA* **92**, 3566-3570 (1995)
- 62. S. Amatschek, E. Kriehuber, W. Bauer, B. Reininger, P. Meraner, A. Wolpl, N. Schweifer, C. Haslinger, G. Stingl, D. Maurer, Blood and lymphatic endothelial cell-specific differentiation programs are stringently controlled by the tissue environment. *Blood* **109**, 4777-4785 (2007)
- 63. J. Keuschnigg, S. Karinen, K. Auvinen, H. Irjala, J. P. Mpindi, O. Kallioniemi, S. Hautaniemi, S. Jalkanen, M. Salmi, Plasticity of blood- and lymphatic endothelial cells and marker identification. *PLoS One* **8**, e74293 (2013)
- 64. N. Kilic, L. Oliveira-Ferrer, S. Neshat-Vahid, S. Irmak, K. Obst-Pernberg, J. H. Wurmbach, S. Loges, E. Kilic, J. Weil, H. Lauke, D. Tilki, B. B. Singer, S. Ergun, Lymphatic reprogramming of micro vascular endothelial cells by CEA-related Cell Adhesion Molecule-1 via interaction with VEGFR-3 and Prox1. *Blood*, (2007)

- M. Francois, A. Caprini, B. Hosking, F. Orsenigo, D. Wilhelm, C. Browne, K. Paavonen, T. Karnezis, R. Shayan, M. Downes, T. Davidson, D. Tutt, K. S. Cheah, S. A. Stacker, G. E. Muscat, M. G. Achen, E. Dejana, P. Koopman, Sox18 induces development of the lymphatic vasculature in mice. *Nature* 456, 643-647 (2008)
- C. Norrmen, K. I. Ivanov, J. Cheng, N. Zangger, M. Delorenzi, M. Jaquet, N. Miura, P. Puolakkainen, V. Horsley, J. Hu, H. G. Augustin, S. Yla-Herttuala, K. Alitalo, T. V. Petrova, FOXC2 controls formation and maturation of lymphatic collecting vessels through cooperation with NFATc1. *J Cell Biol* 185, 439-457 (2009)
- 67. T. Karnezis, R. Shayan, C. Caesar, S. Roufail, N. C. Harris, K. Ardipradja, Y. F. Zhang, S. P. Williams, R. H. Farnsworth, M. G. Chai, T. W. Rupasinghe, D. L. Tull, M. E. Baldwin, E. K. Sloan, S. B. Fox, M. G. Achen, S. A. Stacker, VEGF-D promotes tumor metastasis by regulating prostaglandins produced by the collecting lymphatic endothelium. *Cancer Cell* 21, 181-195 (2012)
- 68. M. Seo, S. Lee, J. H. Kim, W. H. Lee, G. Hu, S. J. Elledge, K. Suk, RNAi-based functional selection identifies novel cell migration determinants dependent on PI3K and AKT pathways. *Nature communications* **5**, 5217 (2014)
- 69. C. D. Nobes, A. Hall, Rho, rac, and cdc42 GTPases regulate the assembly of multimolecular focal complexes associated with actin stress fibers, lamellipodia, and filopodia. *Cell* **81**, 53-62 (1995)
- 70. E. Fagiani, P. Lorentz, L. Kopfstein, G. Christofori, Angiopoietin-1 and -2 exert antagonistic functions in tumor angiogenesis, yet both induce lymphangiogenesis. *Cancer Res* **71**, 5717-5727 (2011)
- T. Holopainen, P. Saharinen, G. D'Amico, A. Lampinen, L. Eklund, R. Sormunen, A. Anisimov, G. Zarkada, M. Lohela, H. Helotera, T. Tammela, L. E. Benjamin, S. Yla-Herttuala, C. C. Leow, G. Y. Koh, K. Alitalo, Effects of angiopoietin-2blocking antibody on endothelial cell-cell junctions and lung metastasis. *J Natl Cancer Inst* 104, 461-475 (2012)
- 72. T. Majima, K. Takeuchi, K. Sano, M. Hirashima, D. P. Zankov, M. Tanaka-Okamoto, H. Ishizaki, J. Miyoshi, H. Ogita, An Adaptor Molecule Afadin Regulates Lymphangiogenesis by Modulating RhoA Activity in the Developing Mouse Embryo. *PLoS One* **8**, e68134 (2013)
- 73. W. S. Chen, Z. Cao, S. Sugaya, M. J. Lopez, V. G. Sendra, N. Laver, H. Leffler, U. J. Nilsson, J. Fu, J. Song, L. Xia, P. Hamrah, N. Panjwani, Pathological lymphangiogenesis is modulated by galectin-8-dependent crosstalk between Podoplanin and integrin-associated VEGFR-3. *Nat Commun* 7, 11302 (2016)
- 74. L. N. Cueni, M. Detmar, Galectin-8 interacts with Podoplanin and modulates lymphatic endothelial cell functions. *Exp Cell Res* **315**, 1715-1723 (2009)
- 75. Q. Zeng, Z. Wu, H. Duan, X. Jiang, T. Tu, D. Lu, Y. Luo, P. Wang, L. Song, J. Feng, D. Yang, X. Yan, Impaired tumor angiogenesis and VEGF-induced pathway in endothelial CD146 knockout mice. *Protein & cell* 5, 445-456 (2014)
- N. Jouve, N. Despoix, M. Espeli, L. Gauthier, S. Cypowyj, K. Fallague, C. Schiff, F. Dignat-George, F. Vely, A. S. Leroyer, The involvement of CD146 and its novel ligand Galectin-1 in apoptotic regulation of endothelial cells. *J Biol Chem* 288, 2571-2579 (2013)

- 77. T. Jiang, J. Zhuang, H. Duan, Y. Luo, Q. Zeng, K. Fan, H. Yan, D. Lu, Z. Ye, J. Hao, J. Feng, D. Yang, X. Yan, CD146 is a coreceptor for VEGFR-2 in tumor angiogenesis. *Blood* **120**, 2330-2339 (2012)
- 78. E. Salomonsson, V. L. Thijssen, A. W. Griffioen, U. J. Nilsson, H. Leffler, The anti-angiogenic peptide anginex greatly enhances galectin-1 binding affinity for glycoproteins. *J Biol Chem* **286**, 13801-13804 (2011)
- 79. Y. K. Hong, B. Lange-Asschenfeldt, P. Velasco, S. Hirakawa, R. Kunstfeld, L. F. Brown, P. Bohlen, D. R. Senger, M. Detmar, VEGF-A promotes tissue repair-associated lymphatic vessel formation via VEGFR-2 and the alpha1beta1 and alpha2beta1 integrins. *FASEB J.* **18**, 1111-1113 (2004)
- 80. N. C. Johnson, M. E. Dillard, P. Baluk, D. M. McDonald, N. L. Harvey, S. L. Frase, G. Oliver, Lymphatic endothelial cell identity is reversible and its maintenance requires Prox1 activity. *Genes Dev* 22, 3282-3291 (2008)
- 81. G. Oliver, R. S. Srinivasan, Endothelial cell plasticity: how to become and remain a lymphatic endothelial cell. *Development* **137**, 363-372 (2010)
- 82. M. Groger, H. Niederleithner, D. Kerjaschki, P. Petzelbauer, A previously unknown dermal blood vessel phenotype in skin inflammation. *J Invest Dermatol* **127**, 2893-2900 (2007)
- 83. U. Fiedler, S. Christian, S. Koidl, D. Kerjaschki, M. S. Emmett, D. O. Bates, G. Christofori, H. G. Augustin, The Sialomucin CD34 Is a Marker of Lymphatic Endothelial Cells in Human Tumors. *Am J Pathol* **168**, 1045-1053 (2006)
- 84. R. S. Srinivasan, N. Escobedo, Y. Yang, A. Interiano, M. E. Dillard, D. Finkelstein, S. Mukatira, H. J. Gil, H. Nurmi, K. Alitalo, G. Oliver, The Prox1-Vegfr3 feedback loop maintains the identity and the number of lymphatic endothelial cell progenitors. *Genes Dev* 28, 2175-2187 (2014)
- 85. I. Fischer, S. Schulze, C. Kuhn, K. Friese, H. Walzel, U. R. Markert, U. Jeschke, Inhibiton of RET and JAK2 signals and upregulation of VEGFR3 phosphorylation in vitro by galectin-1 in trophoblast tumor cells BeWo. *Placenta* **30**, 1078-1082 (2009)
- 86. P. A. Carroll, E. Brazeau, M. Lagunoff, Kaposi's sarcoma-associated herpesvirus infection of blood endothelial cells induces lymphatic differentiation. *Virology* **328**, 7-18 (2004)
- 87. Y. K. Hong, K. Foreman, J. W. Shin, S. Hirakawa, C. L. Curry, D. R. Sage, T. Libermann, B. J. Dezube, J. D. Fingeroth, M. Detmar, Lymphatic reprogramming of blood vascular endothelium by Kaposi sarcoma-associated herpesvirus. *Nat Genet.* **36**, 683-685 (2004)
- 88. F. T. Liu, R. J. Patterson, J. L. Wang, Intracellular functions of galectins. *Biochim Biophys Acta* **1572**, 263-273 (2002)
- 89. T. V. Petrova, T. Makinen, T. P. Makela, J. Saarela, I. Virtanen, R. E. Ferrell, D. N. Finegold, D. Kerjaschki, S. Yla-Herttuala, K. Alitalo, Lymphatic endothelial reprogramming of vascular endothelial cells by the Prox-1 homeobox transcription factor. *Embo J* 21, 4593-4599 (2002)
- 90. Y. K. Hong, N. Harvey, Y. H. Noh, V. Schacht, S. Hirakawa, M. Detmar, G. Oliver, Prox1 is a master control gene in the program specifying lymphatic endothelial cell fate. *Dev.Dyn.* **225**, 351-357 (2002)

- 91. J. L. Hor, P. G. Whitney, A. Zaid, A. G. Brooks, W. R. Heath, S. N. Mueller, Spatiotemporally Distinct Interactions with Dendritic Cell Subsets Facilitates CD4+ and CD8+ T Cell Activation to Localized Viral Infection. *Immunity* 43, 554-565 (2015)
- 92. R. A. Irizarry, B. M. Bolstad, F. Collin, L. M. Cope, B. Hobbs, T. P. Speed, Summaries of Affymetrix GeneChip probe level data. *Nucleic Acids Res* **31**, e15 (2003)
- 93. M. E. Ritchie, B. Phipson, D. Wu, Y. Hu, C. W. Law, W. Shi, G. K. Smyth, limma powers differential expression analyses for RNA-sequencing and microarray studies. *Nucleic Acids Res* **43**, e47 (2015)
- 94. W. Huber, V. J. Carey, R. Gentleman, S. Anders, M. Carlson, B. S. Carvalho, H. C. Bravo, S. Davis, L. Gatto, T. Girke, R. Gottardo, F. Hahne, K. D. Hansen, R. A. Irizarry, M. Lawrence, M. I. Love, J. MacDonald, V. Obenchain, A. K. Oles, H. Pages, A. Reyes, P. Shannon, G. K. Smyth, D. Tenenbaum, L. Waldron, M. Morgan, Orchestrating high-throughput genomic analysis with Bioconductor. *Nat Methods* 12, 115-121 (2015)
- 95. D. J. McCarthy, G. K. Smyth, Testing significance relative to a fold-change threshold is a TREAT. *Bioinformatics* **25**, 765-771 (2009)
- 96. C. Lottaz, X. Yang, S. Scheid, R. Spang, OrderedList--a bioconductor package for detecting similarity in ordered gene lists. *Bioinformatics* **22**, 2315-2316 (2006)
- 97. T. J. Gambino, S. P. Williams, C. Caesar, D. Resnick, C. J. Nowell, R. H. Farnsworth, M. G. Achen, S. A. Stacker, T. Karnezis, A Three-Dimensional Lymphatic Endothelial Cell Tube Formation Assay to Identify Novel Kinases Involved in Lymphatic Vessel Remodeling. *Assay and drug development technologies* **15**, 30-43 (2017)
- 98. A. F. Odell, M. Hollstein, S. Ponnambalam, J. H. Walker, A VE-cadherin-PAR3-alpha-catenin complex regulates the Golgi localization and activity of cytosolic phospholipase A(2)alpha in endothelial cells. *Molecular biology of the cell* 23, 1783-1796 (2012)
- N. C. Harris, N. Davydova, S. Roufail, S. Paquet-Fifield, K. Paavonen, T. Karnezis, Y. F. Zhang, T. Sato, J. Rothacker, E. C. Nice, S. A. Stacker, M. G. Achen, The propeptides of VEGF-D determine heparin binding, receptor heterodimerization, and effects on tumor biology. *J Biol Chem* 288, 8176-8186 (2013)
- G. Finak, N. Bertos, F. Pepin, S. Sadekova, M. Souleimanova, H. Zhao, H. Chen,
   G. Omeroglu, S. Meterissian, A. Omeroglu, M. Hallett, M. Park, Stromal gene expression predicts clinical outcome in breast cancer. *Nat Med* 14, 518-527 (2008)
- 101. X. J. Ma, S. Dahiya, E. Richardson, M. Erlander, D. C. Sgroi, Gene expression profiling of the tumor microenvironment during breast cancer progression. *Breast Cancer Res* **11**, R7 (2009)

Acknowledgments: We wish to thank Dr Maria Macheda and Ms Sally Roufail for technical assistance, Daniel Thomas and Yanny Handoko for screening assistance, Kaushalya Amarasinghe for bioinformatics assistance, and Pritinder Kaur (Peter MacCallum Cancer Centre for providing primary human dermal fibroblasts. We also thank Janna Taylor for assistance in generating the figures. Funding: This work was funded partly by a Program Grant from the National Health and Medical Research Council of Australia (NHMRC). SAS and MGA are supported by Senior Research Fellowships from the NHMRC. SAS acknowledges the support of the Pfizer Australia Fellowship. SPW received a Doctoral Research Scholarship from the National Breast Cancer Foundation. NCH and RL received a Melbourne Research Scholarship from the University of Melbourne. GKS is supported by an NHMRC Program Grant and Fellowship. SNM and LC are supported by Future Fellowships from the Australian Research Council (ARC). The Victorian Centre for Functional Genomics is funded by the Australian Cancer Research Foundation (ACRF), the Victorian Department of Industry, Innovation and Regional Development (DIIRD), the Australian Phenomics Network supported by funding from the Australian Government's Education Investment Fund through the Super Science Initiative, the Australasian Genomics Technologies Association, the Brockhoff Foundation and the Peter MacCallum Foundation. Author contributions: Conceptualization, SPW, AFO, TK, KJS, MGA, SAS; Data Curation, CMG, SPW; Funding Acquisition, MGA, SAS; Investigation, SPW, AFO, SPF, NCH, RHF, RL, AW, JLG, SFL, EAT, NIB, DR, GKS; Methodology, SPW, AFO, TK, SPF, GKS; Resources, CRW, BMH, SBF, SM, KJS; Software, CMG, CJN, JL; Supervision, LC, CRW, BMH, SNM, SM, KJS, MGA, SAS; Visualization, SPW, AFO, RHF; Writing - Review & Editing, SPW, SAS, AFO, RHF, MGA, GKS, SM. Competing Interests: SAS and MGA are shareholders in Opthea Ltd., a company involved in developing therapeutics and diagnostics to vascular targets. All other authors declare no financial conflict of interest. Data and materials availability: Annotated primary siRNA screen data: Pubchem, accession number AID 1159578. Primary screen scratch assay images: Figshare, doi:10.6084/m9.figshare.3980184. Secondary deconvolution siRNA screen data: Pubchem, AID 1159579. Tertiary siRNA screen migration data: PubChem, AID 1159618. Tertiary siRNA screen morphology data: PubChem AID1159617. Tertiary screen morphology images: Figshare; doi:10.6084/m9.figshare.c.3150637. The mouse LN microarray deposited the **GEO** database stromal data are in (http://www.ncbi.nlm.nih.gov/geo/) under the accession code GSE84284.

# **Figure Legends**

Fig. 1. Overview of lymphatic endothelial cell migration screen and analyses

(A) HDLEC monolayers were transfected with CDC42 or CDH5 siRNA pools (as positive controls) and subjected to the scratch wounding assay. Values represent the percentage migration relative to the mean of mock-transfected (Control) cells. Scale bar, 500 μm. (B) Plot of the primary screen results for each siRNA pool. Migration scores plotted on the x-axis are expressed as robust z scores. Each point represents the average of two replicate wells per gene-specific siRNA pool. Results with |robust z score| > 2 (dashed vertical lines) were considered as "Accelerated" or "Impaired" "migration candidates", and those with cell density <60% of the median per field (dashed horizontal line) were classified as "Low Cell Count". (C) Schematic representation of the relationships between datasets, experimentally-derived gene lists and specific analyses within this study. Blue boxes, complete datasets. Red boxes, summaries of the siRNA

# Fig. 2. Functional categorization of highly-validated genes that promote lymphatic endothelial cell migration

are indicated. MIARE, Minimum Information About an RNAi Experiment.

migration screens. Other boxes, specific analyses. Bullet points, the gene list input into

the given analysis or Data File. The gene list size and the Data File containing the results

Annotation of the 154 "highly-validated" candidates into groups reflecting their functional role in the cell, based on literature and text-mining and Metacore analysis (fig. S4, and Data Files S5, S6). Connecting lines represent protein–protein interactions.

# Fig. 3. Morphological changes induced by siRNAs targeting validated candidate genes

(A) Fluorescent microscopy images of cells stained with Celltracker Green (whole-cell) and Phalloidin CF555 (filamentous actin) were subjected to automated high content analysis of cellular regions. Green lines delineate valid cell segmentation boundaries. Scale bar, 250 μm. (B) Unsupervised clustering of candidate genes and cell morphological parameters (such as size, shape, actin intensity) allows identification of genes that regulate similar aspects of cell morphology. Selected example candidates are indicated below the heatmap. (C) Examples of morphological changes observed following transfection with siRNA pools in cluster 2 (see also fig. S5). Scale bar, 250 μm. (D) Comparison of four distinguishing morphological parameters across morphology clusters. A schematic diagram of representative morphology, with actin in orange, is depicted for each cluster.

# Fig. 4. Evaluation of highly-validated candidate migration genes in HMBECs

Migration was assessed in HMBECs and HDLECs transfected with siRNA pools targeting the 154 "highly-validated" candidate genes. (A) Dotplot comparing the migration screen results in HDLECs (x-axis) compared to HMBECs (y-axis). Each datapoint represents a gene-specific siRNA pool, represented as the average migration score of two biological replicates (each comprising technical duplicate wells), relative to mock-transfected controls. Results with migration scores below 0.65 (dotted lines) in HDLECs and/or HMBECs were classified into the indicated categories (quadrants). (B) Migration phenotypes resulting from transfection of HMBECs or HDLECs with the indicated siRNA pools. Cells are labelled with Celltracker Green. Scale bar, 500 μm. (C)

Lists of the genes identified as having LEC-dominant and BEC-dominant effects on migration. Inset numbers represent the morphology clusters as defined in Fig. 3. (**D**) Heatmap of HMBEC morphology parameters. Gene and parameter order was not subjected to hierarchical clustering, but was kept the same as in Fig. 3B to highlight the similarities and differences in morphological phenotypes observed between the two cell types. Selected example candidates are labelled below the heatmap. (**E**) Comparison of the morphological changes that are induced by transfection of HMBECs and HDLECs with an siRNA pool targeting *LPL* (see also fig. S7C). Scale bar, 250 µm.

#### Fig. 5. The endothelial cell migratome

The 68 Common EC migration candidates and 20 LEC Dominant candidates were analysed for protein-protein interactions, identifying two-step pathways between many validated EC migration genes. Migration candidates are colour-coded to match Fig. 4, A and C. Coloured boxes with dashed outlines indicate functional categories.

# Fig. 6. Overlap between migration candidate genes and genes differentially-expressed during lymphatic remodeling in vivo

(A) Immunofluorescence staining of LNs from uninfected control mice (Day 0) and 5 days after subcutaneous HSV-1 infection (Day 5), to identify lymphatic vessels (LYVE-1), high endothelial venules (PNAd) and all other endothelium (CD31). Scale bar, 200 µm. (B) The list of genes differentially expressed (HSV-1 day 6 compared to day 0) in LN LECs in the microarray analysis was compared to the "expanded migration candidate" list from the primary siRNA screen (excluding "Low Cell Count" genes) to

determine the number and significance of overlapping genes. Significance of overlap was defined against a simulated null distribution derived from 10,000 random pairs of gene lists of equivalent size as described in Materials and Methods. (C) Venn diagram of the number of input and overlapping genes from the analysis in (B). \*\*\*Empirical P value < 0.001; hypergeometric P value = 0.0078 (D) Filtering of differentially-expressed genes into cell-selective and shared categories, and comparison of these gene lists to the "expanded migration candidate" list. Empirical P values were determined according to simulated null distributions as in (B); hypergeometric P values are in footnote b. (E) Venn diagram of the number of overlapping genes identified between the different categories of differentially-expressed genes in (D) with genes identified in the primary siRNA screen. Intersections are exclusive of one another and colour-coded to match (D). \*P < 0.05, \*\*P < 0.01 empirical P values. (F) Venn diagram of overlapping genes between those differentially-expressed in dermal LECs during CHS (24 h compared to unstimulated) and the "expanded migration candidate" list. \*P < 0.05 empirical P value; hypergeometric P value = 0.0547.

Fig. 7. Galectin-1 regulates lymphatic endothelial cell migration in vitro and in vivo (A and B) Western blotting for Gal-1 in cultured HDLECs and HMBECs (A), and in HDLECs transfected with LGALSI siRNA pool (B). "Control" indicates mocktransfected cells in (B) and (D-G); non-targeting siRNA in (C). (C) Quantitation of Gal-1 knockdown by Western blotting. Mean ± SEM of n = 4 independent experiments; \*\*\*\*P < 0.0001 by Student's t test. (D) Tube network formation under Collagen I gel by HDLECs. Scale bar, 250 μm. Mean ± SEM of three independent experiments shown; \*P

< 0.05 by Student's t test. (E) HDLECs with or without LGALS1 knockdown were grown on a confluent fibroblast monolayer before CD31 and LYVE1immunofluorescence was performed to visualise HDLECs and smooth muscle actin (SMActin) to stain fibroblasts. Scale bar, 250 µm. (F, G) Tubule networks from (E) were quantified by the parameters indicated. Mean  $\pm$  SEM of three independent experiments; (F) \*P < 0.05 by ANOVA with Tukey post-hoc test; (G) P = 0.05 by Student's t test. (H) Immunofluorescence for LYVE-1 (lymphatics), and CD146 (blood vessels) on mouse ears injected with the indicated proteins in Matrigel, with or without the Gal-1 inhibitor Anginex. Scale bar, 250  $\mu$ m. Lymphatic vessel width and density was quantitated. n = 9 mice with 9-18 ears per condition across two independent experiments. Mean  $\pm$  SEM; \*P < 0.05, \*\*P < 0.01by ANOVA with Tukey post-hoc test. (I) Immunohistochemistry on serial sections of human LN. White arrows: lymphatic vessel (LV). Black arrowhead: blood vessel (BV). Scale bar, 50 µm. (J) Bioinformatic interrogation of two published gene expression datasets (100, 101) for LGALS1 expression in normal tissues and cancer stroma. Central line, median; box, interquartile range; whiskers, 90/10 percentiles; dots, minimum/maximum; P values determined in Oncomine using two-sample t test.

# Fig. 8. Gal-1 signalling maintains lymphatic endothelial cell phenotype (A) HDLECs transfected with LGALSI siRNA pools were serum-starved before stimulation with VEGFA (20 ng/ml) then analysed by immunoblotting. Control, non-targeting siRNA; Src, Src family kinases. (B) Quantification of phospho (p)-VEGFR2, p-ERK 1/2 and p-Akt bands in (A), normalised to the total respective protein and expressed relative to unstimulated Control-transfected cells. Mean $\pm$ SEM; n = 3-6 independent

experiments; \*P < 0.05, \*\*P < 0.01 by ANOVA with Tukey post-hoc test. (**C**) Quantification of total VEGFR3 bands in (A) normalised to loading control; mean  $\pm$  SEM shown; n = 3 independent experiments; \*P < 0.05 by Student's t test. (**D**) 24 h following scratch-wounding, siRNA-treated HDLECs were examined by immunofluorescence for indicated proteins; nuclei were counterstained with Hoechst 33342 (Hoechst). Scale bar, 250  $\mu$ m. For quantification see fig. S12A. (**E**,**F**) Lysates of HDLECs transfected as indicated were analysed after 72 h by Western blotting for LEC, BEC or common endothelial lineage marker proteins. (**G**) Quantitation of Western blot analyses of respective LEC and BEC marker proteins in (E,F), normalised to loading control. Mean  $\pm$  SEM; VEGFR2 n = 8 independent experiments; VEGFR3 n = 10 independent experiments; CD146 n = 6 independent experiments; CEACAM1 n = 5 independent experiments; Podoplanin n = 3 independent experiments; Prox1 n = 5 independent experiments. \*P < 0.05, \*\*P < 0.01 by ANOVA with Dunnett post-hoc test.